Responses to the interactive comment on *"Measuring dynamic wake characteristics with nacelle mounted LiDAR systems" by Inga Reinwardt et al., manuscript number: wes-2019-89*

Responses to the referee: Vasilis Pettas (pettas@ifb.uni-stuttgart.de)
Received and published: 04.02.2020

1. General comments

Thank you very much for the detailed and helpful comments on the paper. We appreciate the work of reviewing it and believe that the quality of the paper significantly gained from the comments.

In the following, we respond to all comments in detail. Particular focus is given to the main comment on more quantitative results and their precise description by introducing further graphs and explanations. The uncertainties are discussed more in detail as well as the data filtering procedure.

2. Specific comments

Title

Is the title reflecting the content? Maybe use a more descriptive one, like for instance: "Calibrating a DWM model with measurements of dynamic wake characteristics using nacelle mounted lidar systems"?

Response*:* A more precise title is reasonable and adjusted to: DWM model calibration using nacelle mounted lidar systems.

Abstract

Specify the objectives of the paper clearly, not only the campaign.
What do we learn by reading the paper?
I would suggest removing lines 4 - 5 as no discussion on the optimization procedure is done in the paper itself.

Response*:* Line 4-5 were removed.

Introduction

L 13: Engineering models like the Frandsen model are intended to calculate mainly the wake deficit and shape and not the wake induced turbulence. It should be clearly stated.

Response*:* As far as we know, the Frandsen model is commonly used in the industry to calculate the wake induced turbulence and is also recommended in the IEC guideline. What kind of model do you mean here?

L 24: What is meant by 2D wind field here?
The lidar can measure 1D (LOS direction only) and 3D in terms of space (have the pulsed technology with range gates). Please clarify.

Response*:* The text passage was rephrased to: *"Especially, the so-called scanning LiDAR systems offer great potential for detailed wake analysis. These LiDARs are capable of scanning a three-dimensional wind field, so that the line of sight (LOS) wind speed can be measured subsequently at different positions in the wake, thus enabling the detection of the wake meandering as well as the shape of the wind speed deficit in the MFR."*

At the end of the introduction a paragraph should be added stating clearly the objectives of the paper. A small reference on the content and structure of the following sections could also make the work easier to follow.

Response*:* A clear outline of the objectives was added and a small overview of the structure of the following sections was given:

"Thus, a detailed comparison of the predicted degradation of the wind speed deficit between the DWM model and the measurement results is possible. Furthermore, the collected LiDAR measurements are used to recalibrate the DWM model, so that the wake degradation can be modeled more precisely. As a consequence, the calculation of the loads as well as the energy yield of the wind farm can be improved. The remaining document is arranged as follows: in Section 2, the investigated wind farm and the installed measurement equipment are described in detail. Afterwards, in Section 3, an explanation of the data processing and filtering of the measurement results is given. Sections 4, 5, and 6 focus on the description of the theoretical background and a hands-on implementation of the DWM model is introduced. Based on the outlined measurement results, a recalibration of the defined degradation of the wind speed deficit in the DWM model is proposed in Section 6. A summary of the measurement results can be found in Section 7 and a comparison to the original DWM model as well as the recalibrated version is presented in Section 8. Eventually, all findings are concluded in Section 9."

Wind farm

L 67-68: As I understand load measurements are not used in the study, what is the relevance of mentioning the load sensors here

Response*:* The load measurements should be used in a subsequent publication and should be used to further verify the recalibration of the DWM model. A hint to future objectives is added.

L 69: LiDAR system of WTG 1 is installed inside the nacelle and measures through a hole in the rear wall: This is an interesting and uncommon setup. Are there any limitations or benefits using this set up? It could be useful information for future campaign

Response*:* Mounting the device on top of the nacelle of WTG 1 is not possible, as the area is occupied by a recuperator. The reason and the limitations that accompany it are complemented.

L 70: A nacelle mounted GPS is mentioned for the nacelle yaw position tracking. What is the uncertainty of such a system? Did you correlate it with the high frequency SCADA data for nacelle direction?

Is there any data filtering based on SCADA or gps nacelle position in order to make sure that the turbines were not yawing often during the accepted time intervals?

Response*:* The differential GPS system measures in centimetre range. A comparison between the SCADA data nacelle direction has been done. This comparison has shown that the measured nacelle direction of the SCADA system has a non-negligible offset of more than 10° at some turbines. This error in measuring the nacelle direction occurs frequently at common wind turbines, wherefore we decided to install the GPS systems. The GPS systems are used to ensure that the turbines are not yawing during the used time intervals. This is also mentioned in Section 4.

L 78 - 80: The Richardson number is mentioned here. It is not mentioned how it was used to filter the data or how it is used in general in the study.
Stability is only mentioned again in L 216 where it is stated that it is not considered. Am I missing something?
L 79:State the heights of measurements used for the calculation of the Richardson number
Response*:* First, we divided the data set into stable and instable measurements, but in the end, we used all data sets for the recalibration of the DWM model. Therefore, the Richardson number calculation was removed. Furthermore, in L216, in the description of the DWM-Keck model, it is explicitly pointed out that no atmospheric stability is included in the model, as the referred author of this model version developed a model with atmospheric stability included and to clarify that this approach is not used here.

How many rays are used in each pulse for the campaign?
Response*:* The pulse repetition rate of the LiDAR system is 15 kHz and the ray update rate is about 1Hz, so it averages over approximately 15,000 pulses (depending on the atmospheric conditions). The sample frequency is 100 MHz. Considering the speed of light, we get a point length of 1.5 m. The range gate length is 30 m, thus 20 points are used per range gate. This explanation was also added to the paper.

Are the SCADA data used 10min averages or high frequency?
Response*:* The SCADA data is only used to determine if the turbine operates under normal power production conditions and to affirm no yaw misalignment. For this purpose, the statistics of the 10-min time series are used. All other data filtering is done with the metmast and the GPS systems.

L 73-88: A lot of information in this paragraph. Would be clearer to add a table with all the filtering as well as the amount of total data and data kept after filtering. This way it will be easier to identify sources of bad measurements and provide a condensed overview.
Response*:* The paragraph was restructured, and a workflow was added to clarify the filtering procedure. The amount of data after filtering has already been given in Table 2 in the results section.

L 85-88: Give more details on the final setup of the lidar campaign. What was the sampling rate per scan/ray? Which range gates were used (as 750m exceeds the distance of the downwind turbines and usually this type of devices cannot measure below 50-100m)? Exact information on the campaign can be very useful for future research.
Response*:* The sampling rate as well as the range gates were added in the section (see also previous comment). The range gates used for the validation of the DWM model and the recalibration can vary between each used time series because not all range gates fulfill the filtering criteria. Nevertheless, the used range gates for all data sets are illustrated in Figures 6, 7, and 8. Further distances, which are not illustrated in these graphs, are not considered.

L89-94: Is there any uncertainty in that? According to the misalignment of the nacelle to the main direction, the tilt or yaw flows and the lidar angle, the uncertainty can be significant. Is there a way to quantify that? What are the angles used and how small are they?
Response*:* A discussion and estimation of the error made by yaw misalignments was supplemented as follows: *"…if there is yaw misalignment, this could have an impact on the overall results. To decrease the uncertainties based on yaw misalignments, the measurement*

data has accordingly been filtered. The yaw misalignment has the biggest impact at the largest scan opening angles, so that a misalignment of 6° at an opening angle of 20° leads to an overestimation of the wind speed of less than 5%.".

Wind speed deficit in MFR calculation

L 107-108: "However… campaign" This is a good example of more concise language and argumentation needed in the paper. What does highly improbable mean (especially when only 1 10min data set is used for some TI bins later on)? What does very robust mean? Please be more specific in the arguments used to validate assumptions.

Response*:* Results of the calculation of the position of the wind speed deficit at 200 m based on the DWM model simulation has been added to clarify the very low probability (*"e.g., the DWM model predicts the wind speed deficit's probability at the horizontal position of 200 m to be $2*10^{-22}$ for an ambient wind speed of 6.5 m/s and an ambient turbulence intensity of 8 %"*).

What is meant by "especially when only 1 10min data set is used for some TI bins later on"? Are you suggesting that too much data is filtered out due to the 200 m criterion? Based on the simulation results given from the DWM model, this is not the case.

L 118-120: Maybe I am missing something, but it is not clear to me how this plausibility check works. Can you explain it more?

Response*:* After averaging the wind speed deficits in the MFR and FFR, the calculated minimum mean wind speed in the MFR is compared to the minimum mean wind speed in the FFR. In theory, the wind speed deficit in the MFR should be more pronounced than the measured one in the FFR. This comparison is used as a plausibility check.

Lidar simulation

This section needs a lot of work, with a lot of missing information. More information is needed in order to ensure reproducibility. How is the lidar simulator working? How are the wind fields created and how is the DWM model incorporated? Are you using Turbsim or Mannbox generator or some other turbulence generator? How is the LOS speed reconstruction done? Do you consider perfect lidar measurements? How are the range gates and probe volume averaging considered?

Response*:* The LiDAR simulations are very simple and basic to ensure that the meandering as well as the wind speed deficit in the MFR could be captured with the used devices and to check if the selected scan pattern is usable. The wind field with wake effects is generated with an in-house Python tool. A detailed description of the model implementation is given in Section 6 and is not repeated here. A hint to the next section has already been given. There, it is explained that the Veers model is used instead of the Mannbox. The simulations assume perfect LiDAR measurements, so that no probe volume averaging is considered and the LiDAR directly measures the horizontal wind speed. The wind field is simulated at midway of the range gate.

L 129-131: This is the only reference through the paper to the optimization study to find an optimal pattern. It results to a simple horizontal scan of 11 equispaced points. It is very general and does not explain the procedure. I think it should either omitted from the paper and only state the used trajectory or add a dedicated section with more details and figures.

Response*:* L129-131 has been rephrased. The LiDAR simulation are only used to check if the scan pattern could be used in the campaign and only manual iteration processes with different angle increments have been carried out. To avoid further misunderstandings, the term "optimization" has been replaced in the description. Graphs with results of simulation and simulated "measurements" are given in Figure 3.

L 136: What does very well mean in this context? Can it be quantified e.g. with error metrics or R^2?
Response*:* The coefficient of determination is given in Figure 3 (R^2=0.93). A hint in the text was added, too.

L 144-146: What does optimal operating conditions mean? Does it mean it operated on max CP, CT which in turn produce the highest deficit? Please be more specific. Maybe a dimensionless CP-CT vs wind speed curve would be useful here but also for the argumentation in L 299 about thrust being constant.
Response*:* Yes, optimal operating conditions means operating at maximum CP, where the highest or most pronounced deficit is generated. CP and CT curves are added in the section "wind farm".

Dynamic wake meandering model
Sections 6.1 and 6.2: Nice, thorough description of the models. Can you explain how you generated the wind fields (tools, models, parameters, discretization) and how you implemented the variations of the DWM models? Is this an in-house tool or a commercial/open source tool? Can the codes be shared with others so that such validations can be repeated with other data sets?
Response*:* The wind fields are generated with an in-house Python tool, as mentioned in Section 6 and described in Section 6.1. The discretization in axial and radial direction for solving the thin shear layer equations is 0.2D and 0.0125. The information was added to the description. The axial induction factor, which is needed for calculating the boundary conditions, cannot be shared because these are confidential data of the turbine manufacturer. All other parameters are given. The source code can be requested by the authors as explained at the end of the paper in the provided section "Code and data availability".

Section 6.3: As stated, the wake induced turbulence in the DWM model is not used in this study. I suggest to remove this section as it does not add something to the purpose of the paper.
Response*:* The section was removed.

L 258-259: What does relatively good agreement mean in this context? Please be more precise and avoid using such expressions.
Response*:* The sentence was rephrased.

The results with high shear and low TI (and vice versa) suggest some kind of stability based filtering in the results. Is this done somehow? Would this be an important parameter on how well the DWM models and the parameter fitting perform?
Response*:* There is no stability filtering included in the results. Previously, a filtering according to atmospheric stability was implemented, but since this drastically decreases the amount of data, it was discarded and only a sorting according to turbulence intensity bins has been carried out. Moreover, the used eddy viscosity description in the DWM model,

which is calibrated, only depends on the turbulence intensity, thus atmospheric stability is only partially and indirectly considered in the model description, which is why a classification into turbulence intensity bins is more valuable in this application.

L 270-271: Can't this (along with the observation that the center of the wake in the MFR is not exactly at the 0 point) correlated to the rotational direction of the rotor too?
Response*:* The movement of the wake is based on the assumption that the wake behaves as a passive tracer in a turbulent ambient wind field, so the movement is driven by large scale turbulences and not by the rotational direction of the rotor. Furthermore, if the displacement would be correlated to the rotational direction of the rotor, this behaviour should be visible in all data sets, which is not the case.

L 277-280: This discussion is interesting and would be more relevant if it could quantify the trade-offs. As mentioned in a previous comment this could fit in the numerical study of the optimization.
Response*:* A quantitative discussion of the possibility of increasing the number of scan points was added: *"According to Equation (18), the meandering is correlated to frequencies lower than approximately 0.028 Hz considering a wind speed of 6.5 m/s and a rotor diameter of 117 m. This means that, considering the Nyquist–Shannon sampling theorem, the scan time must be longer than half of the reciprocal of 0.028 Hz, which results in a necessary scan time of less than 18 s. The scan time for the current usage of 11 scan points is already at about 16 s (depending on the visibility conditions), which is close to the limit of 18 s, so with an increased number of scan points it is no longer ensured that the meandering can be captured."*

L 293-298: and L 305 and L 311-314: The data for bins of TI higher than 12 seem very sparse with 1 or 2 data sets each. Are these sufficient to extract conclusions about the models and fit parameters? I would suggest a more thorough argumentation for using them or removing values higher than 12 from the analysis.
Response*:* The agreement between the measurements and the simulations is already good in the higher turbulence intensity bins, so the recalibration affects only the lower turbulence intensity bins with larger amounts of data, while the influence of the calibration on higher turbulence intensities is negligible. Therefore, it would not make any difference to exclude the data from the model fit. This explanation is added at the end of Section 7.

Table 2: Could it include also shear values? Or maybe a plot can be added showing the joint probabilities of shear and TI. This will help to give a better overview of the conditions to the reader.
Response*:* A scatterplot of shear and TI was added.

Figure 2 is hard to read. I recommend plotting it again with thicker lines and playing with line style, markers and size
Response*:* The authors think that the method description in Figure 2 is sufficient.

L298-301: As mentioned earlier, a CP-CT curve vs wind speed would be more clear for this argument.
Response*:* CP-CT curves were added and referred to.

L 314-318: The argumentation here is weak. More quantitative results are needed and more concise language in order to validate the assumptions.
Response*:* A more detailed description about the uncertainties related to the determination of the ambient conditions as well as a description, why it is acceptable to use the higher turbulence intensity bins for the recalibration (see also comment to line L 293-298: and L 305 and L 311-314 above), was added as follows: *"The farthest distance between the metmast and the measured wind speed with the LiDAR system, which can occur in the analyzed sectors, is about 1200 m. With an ambient wind speed of 6.5 m/s, this leads to a wake advection time of 185 s, thus even at worst conditions, the measured ambient conditions at the metmast should be valid for the measured wakes from the LiDAR system most of the time. Furthermore, there is no complex terrain at the site, so it can be assumed that the conditions do not change with the wind direction. In addition, the agreement between measurements and simulations is already good in the higher turbulence intensity bins, so the recalibration affects only the lower turbulence intensity bins with larger amounts of data, while the influence of the calibration on higher turbulence intensities is negligible (see Figure 14)."*

Comparison between measurements and DWM model simulation
L 323: Which are the distances used in the simulations?
Response*:* As explained, the simulated distances correspond to the center of the range gate.

L 325-326: "However, the wind speed gradient in axial direction is relatively low and almost linear in the observed downstream distances, so that a fair comparison between simulation and measurements is carried out". The phrasing relatively low and almost linear are not making an argument for the assumptions. Please explain why you consider this valid. Moreover, it is not clear what is meant by fair comparison in this context.
Response*:* The following explanation was added: *"The wind speed gradient in axial direction is low and almost linear in the observed downstream distances, so even in the DWM model, the discretization in downstream direction is 23.4 m (equivalent to 0.2D), which is in the same magnitude as the range gate of 30 m. Therefore, a valid comparison between simulation and measurements is carried out."*

L329 Avoid the phrase 'it is obvious',
Response*:* Phrase was removed.

L320-336 In general the analysis here is only descriptive and qualitative. Can the convergence be quantified and the discrepancies of the model to the measurements explained based on their assumptions and detail level?
Response*:* A graph with the RMSE between the simulations and models was added as well as a comparison of the deviations to the measurement uncertainties that are related to yaw misalignments and measuring the LOS wind speed itself.

L 342 How were the simulations performed? What code was used, what type of spatial and temporal discretization? Give more details.
Response*:* A detailed explanation of the simulations is given in Section 6. It is done with an in-house python tool. The spatial and temporal resolution were also added in this section.

L345 It is not clear to me what does this weighting mean. Can you explain it a bit more along with the reasoning?
Response*:* To calculate a mean value of the simulated minimum wind speed and thus allow a comparison with the measurement results collected at two different turbine types, simulations with both turbine types are carried out for each turbulence intensity bin and weighted in accordance with the number of measurement results per turbine listed in Table 2. Thus, for example at the ambient turbulence intensity bin of 4 %, the mean value of the simulated minimum wind speed consists of the sum of the simulated minimum wind speed weighted by 0.451 and 0.549, the weighting factors for WTG1 and WTG2, respectively. Nevertheless, this weighting has only a marginal influence on the overall results, because the axial induction in the considered wind speed range (5 m/s – 8 m/s) is very small for these two turbine types (see also thrust and power curves in Figure 3). A more detailed explanation was also added in the paper.

L 346 It is stated that the calibrated model "coincides very well with the measurements". Can you quantify this improvement by comparing with the level of agreements of the previous models?
Response*:* A graph with the RMSE between measurements and simulations for all turbulence intensity bins was added to provide a better quantification of the improvements.

L 350 - 362 In this paragraph the differences between the models described based on Figure 10. Can you add some explanation on why the models behave differently? What is the driver of this behavior?
Response*:* The difference between the models was explained in detail in Section 6.1 and repeated in Section 8. The DWM-Egmond model and the DWM-Keck model differ in the definition of the boundary conditions for solving the thin shear layer equations as well as the eddy viscosity definition, which is used to calculate the expansion downstream. The DWM-Keck and the recalibrated DWM-Keck-c model differ in the definition of the eddy viscosity. The faster degradation of the wind speed deficit in the recalibrated model version is caused by introducing the function F_{amb} in the eddy viscosity definition in Equation (21) as explained in Section 6.1. The function increases the eddy viscosity for lower turbulence intensities and thus increases the wind speed deficit degradation in downstream direction.

Conclusions
L 366 As commented earlier the part about deriving an optimal scan pattern is not discussed at all through the paper. I would suggest you either add a section on this optimization procedure or remove it from the text.
Response*:* The sentence was rephrased.

L374 comparably good agreement: This is not clear as a conclusion. As stated earlier I think more concise language and quantitative results are needed
Response*:* The sentence was rephrased.

3. Minor comments
Response*:* All minor comments were adopted in the paper.

Responses to the interactive comment on *"Measuring dynamic wake characteristics with nacelle mounted LiDAR systems" by Inga Reinwardt et al., manuscript number: wes-2019-89*

Responses to the referee: Helge Aagaard Madsen (hama@dtu.dk)
Received and published: 25.02.2020

We are delighted for your valuable comments on the paper. Considering your comments leads to a significant improvement of the paper. We thank you a lot for taking the time to review this paper.

Specific comments
Abstract

The sentence: "the formulation of the quasi-steady wake deficit in the DWM model has been adjusted" is not precise.
It´s proposed to describe that it´s the correlation of the impact of ambient turbulent to the eddy viscosity that has been investigated and that an improved correlation function (parameter) has been determined based on the present measurements.

Response: The sentence has been adjusted to: *"Based on the findings from the LiDAR measurements, the impact of the ambient turbulence intensity on the eddy viscosity definition in the quasi-steady deficit has been investigated and, subsequently, an improved correlation function has been determined, resulting in very good conformity between the new model and the measurements."*

2. Wind farm

Line 68:
- What is the instrumentation in the met mast ? Please describe in the paper.

Response: It is equipped with 11 anemometers, two of which are ultrasonic devices, three wind vanes, two temperature sensors, two hygrometers, and two barometers. The sensors are distributed along the whole metmast, but at least one of each is mounted in the upper eight meters. A Figure with the instrumentation and measurement heights was added.

Line 76:
- What type of load measurements and have they been used for DWM simulations on the turbines?

Response: Strain gauges are installed at the three turbines to measure tower bottom, tower top as well as blade edge- and flapwise moments. Unfortunately, the load measurements are not in the scope of this paper but will be introduced in future publications, i.a., to verify the recalibration. A hint that these load measurements are used for further investigations was added.

3. Data filtering and processing

Line 86:

- … "and sorted in accordance with ambient wind speed, ambient turbulence intensity, windshear, atmospheric stability, and wind direction".
    - is it 10 min, mean values that the data are sorted on basis of ?

Response: Yes, the data are filtered based on the 10-min time series statistics from the metmast. The information was added to the manuscript.

4. Wind speed deficit in MFR calculation

Line 119:

- … "In the analysis presented here only results from a horizontal line scan are analyzed, so that no vertical meandering is considered and the measurement results are fitted to a one-dimensional Gaussian curve defined as follows:"
    - In my view this is an important limitation of the experimental set-up. Overall the impact is that the depth or strength of the deficits are smaller than if the 3D location of the deficits was used. The impact can be investigated using a DWM model and simply set the vertical meandering to zero. Please discuss this limitation of the measurement set-up and what impact it has on the final result.

Response: A comparison of the simulated wind speed deficit with the DWM model in the complete MFR and without eliminating the vertical meandering in the wind speed deficit was added. There are only small discrepancies around the center of the wake. Nevertheless, in the comparison between the simulated wind speed deficit and the measured wind speed deficit the vertical meandering is not eliminated, so that in both cases the wind speed deficit is similarly reduced in depth. Naturally, the minimum wake wind speed deficit in the MFR without elimination of the vertical meandering is used for the recalibration, too. To clarify that the vertical meandering is not eliminated in any case, but included in the wind speed deficit, the abbreviation HMFR (horizontal meandering frame of reference) is introduced and used instead of MFR.

Line 137:

- … "After averaging, the plausibility of the results is inspected. If the calculated minimum mean wind speed in the MFR is higher than the minimum mean wind speed in the FFR, it is assumed that the Gauss fit failed and the results are no longer considered.
    - Besides this plausibility check I would propose to show the standard deviation of all the measurement points around the average MFR from the individual scans, just for a few cases. This will give information about how much averaging is behind the final MFR deficits.

Response: The plots for the corresponding turbulence intensities for Figure 6 (HMFR) and 7 (FFR) are given below. The comparison of the turbulence intensity in the HMFR and FFR show a decrease of the two maxima at the turbulence intensity in the HMFR, which is expected due to the transformation to the HMFR. The two maxima do not vanish completely in the HMFR graphs due to the small-scale turbulence, which is related to blade tip and root vortices as well as the wake shear itself. Additionally, the turbulence which is related to the vertical meandering is still included. Furthermore, the ambient turbulence intensity of

11.7% and 2.4% can be seen towards the edges of the curve, where the wake influence decreases.

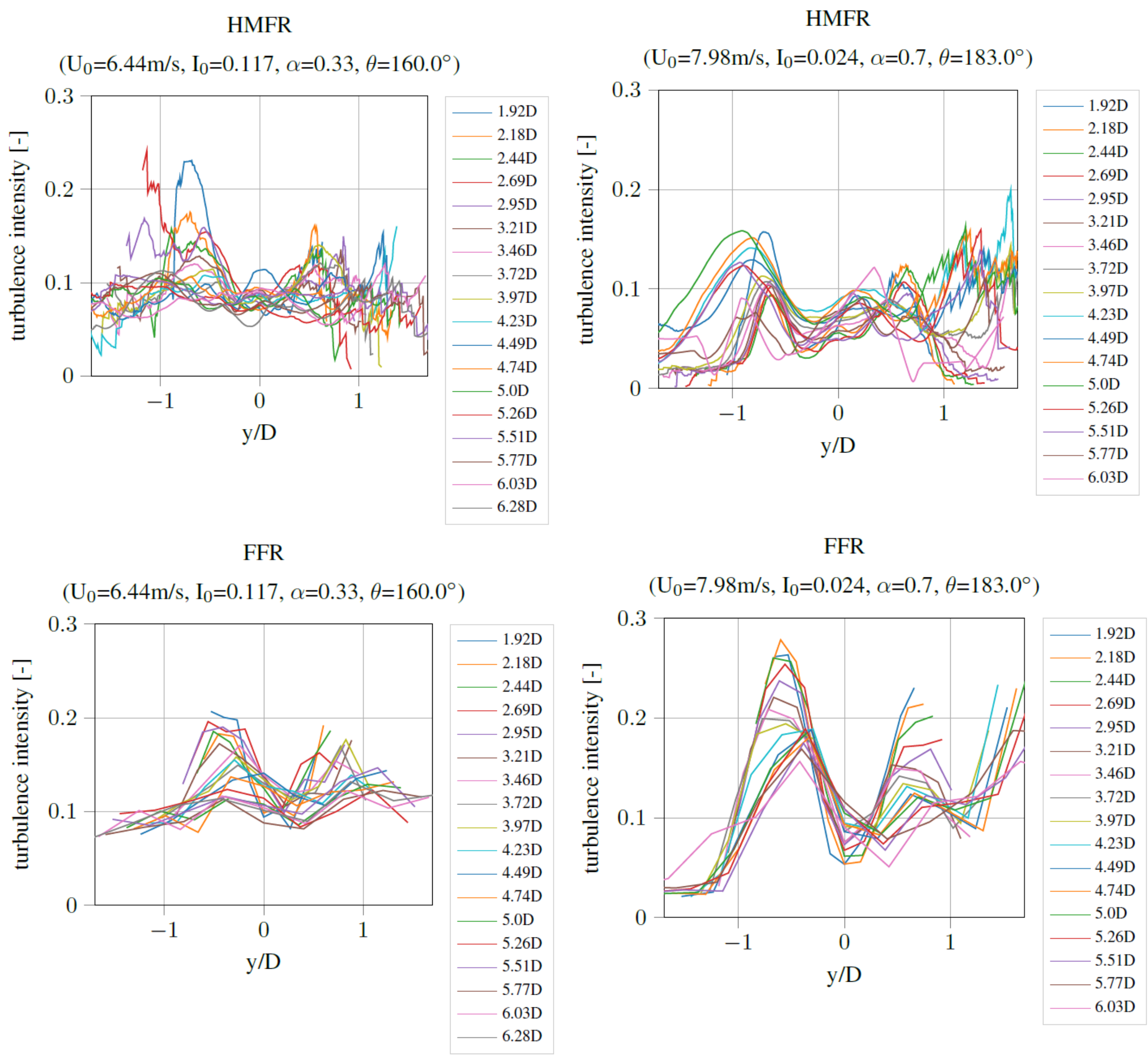

Line 148:

- In figure 2 as I understand the procedure:
  - – shouldn´t the x axis after the interpolation be in y/d units and not in deg. ?. Likewise in Figure 3b.

Response: The label refers to the scan direction, because it is the interpolated scan direction. Nevertheless, it is clearer if the axis is in y/d to correspond to the Figures in section 7. Both graphs were adjusted.

5. LiDAR simulation

Line 159:

- Were the lidar simulations with the DWM model shown in Figure 3 carried out with ambient turbulence or only a meandering turbulence – please specify?

Response: It is the complete DWM model wind field with ambient turbulence. It is specified in the text.

Line 160:

- … "Whenever the wind speed deficit is mentioned in subsequent validations, it implies the neglection of the vertical meandering, which has only a marginal impact on the shape of the wind speed deficit in the FFR.".
    - As the meandering turbulence components scales with 0.8 and 0.5 in horizontal and vertical direction relatively to the streamwise turbulence component I am not convinced that this statement is correct. Please expand on this eventually based on simulations with the DWM model.

Response: A comparison of the simulated wind speed deficit with DWM model in the complete MFR and the HMFR was added (see also response to comment on Line 119).

6. Dynamic wake meandering model

Line 175:

- … "It compares directly to the LiDAR measurements after transforming the measurements into the MFR as explained in the last section".
    - As mentioned above the measured wake deficit might be less sharp (deep) due to neglecting the vertical meandering and due to the averaging of many individual deficits impacted by ambient turbulence.

Response: That is true, although, the DWM model simulations showed that the influence is small. In the comparison between the simulated and the measured wind speed deficit the vertical meandering is also neglected, hence in both cases the wind speed deficit is less deep. Since the sentence seems to be misleading, it was deleted.

Line 189:

- … "The error that inherently comes with this assumption is accommodated by using the wind speed deficit two rotor diameters downstream (beginning of the far-wake area) as a boundary condition for the solution of the thin shear-layer equations. "
    - It might be important to point out here that the eddy viscosity model in the DTU DWM implementation is run from the rotor plane and downstream with the fully expanded wake deficit (eq. 6 and 7) as boundary conditions but where a fit of the deficit at 2D downstream to Actuator Disc simulations determined eq. 8 and the filter function for non- turbulent flow.

Response: The equations are also directly solved from the rotor plane in the implementation here. It is rephrased to:

"The error that inherently comes with this assumption is accommodated by using the wind speed deficit two rotor diameters downstream (beginning of the far-wake area) as a boundary condition for the solution of the thin shear layer equations. The equations are solved directly from the rotor plane by a finite-differences method with a discretization in axial and radial direction of 0.2D and 0.0125D combined with an eddy viscosity (ν_T) closure approach."

In section 6.1.1 DWM-Egmond following sentence was added:

"The filter function as well as Equation 8 are calibrated against actuator disc simulations at a downstream distance of 2D, the beginning of the far-wake area, where the wake is fully expanded (Madsen et al., 2010)."

Line 272:

- … "It shows that for lower turbulence intensities and moderate to high turbine distances the wind speed deficit degradation is too low."
    - Maybe write "was too low in the model version from 2010 – ref J. Sol. Energy Eng., 132, 041 014, 2010." The deviations were the reason to recalibrate the model as presented in the 2013 paper.

Response: This sentence is rephrased to: *"It shows that the wind speed deficit degradation is too low for lower turbulence intensities and moderate to high turbine distances in the model version from Madsen et al. (2010). For this reason, the downstream distance dependent function F_{amb} was introduced into the eddy viscosity description in Larsen et al. (2013)."*

7. Measurement results

Line 289:

- … "The corresponding mean wind speed deficit is illustrated in Figure 6(b)."
    - In order to evaluate what this mean deficit it would be valuable if the standard deviation of the 11 raw measurement points for each scan are shown

Response: The plots of the corresponding turbulence intensities are given in the comment on Line 137.

Line 310:

- … "The reason is probably the wake of other turbines in the wind farm".
    - It could also be due to wake rotation as seen in 3D CFD rotor simulations in sheared inflow. It shows that high velocity flow at one side of the rotor is rotated down towards the ground and the opposite on the other side of the turbine.

Response: If it is due to wake rotation, shouldn't the wind speed on the right edge of the deficit be higher than the ambient wind speed from the metmast? Currently, the wind speed agrees with the ambient wind speed.

Line 323:

- … "In this range both turbines operate under optimal and most efficient conditions resulting in maximum energy output from the wind. The thrust coefficient is constant in this region. Therefore, the axial induction and the wind speed deficit normalized by the turbine's inflow wind speed are also expected to be constant for similar ambient conditions over this wind speed range."
    - Its mentioned ".. expected to be constant". What is actually used in the DWM simulations ?
    - Further down at line 368 is mentioned : ".. that the axial induction of both turbines is slightly different under partial load conditions." So is the detailed aero loading of each of the two turbines are simulated ?

Response: DWM model simulations for the single turbulence intensity bins and both turbine types are carried out and the same axial induction is applied over the whole wind speed range. That means, each turbine type is modelled separately and all turbulence intensity bins are simulated. The sentence is rephrased as follows: *"DWM model simulations were carried out for both turbine types, since the axial induction of both turbines is slightly different under partial load conditions. To calculate a mean value of the simulated minimum wind speed and thus allow a comparison with the results in Figure 12, simulations with both turbine types are carried out for each turbulence intensity bin and weighted in accordance with the number of measurement results per turbine listed in Table 2.".*

8. Comparison between measurements and DWM model simulation

Line 358:

- "For lower turbulence intensities and higher distances (greater than 3D) there is a relatively large discrepancy between measurements and simulations. A similar observation was made in Larsen et al. (2013)."
    - This comment was on the model before the recalibration so it should be deleted if pointing to the "DWM-Egmond model"

Response: It is rephrased to: *"A similar observation was made in Larsen et al. (2013) with the model version in Madsen et al. (2010). Aiming at the adjustment of the simulated degradation of the wind speed deficit in Larsen et al. (2013) for cases like the one presented here, the DWM model has been recalibrated…"*
The sentence is not deleted here, because it should be pointed out that the method of recalibration is similar to the one in Larsen et al. (2013).

Line 362

- As concerns the results in Figure 10 and Figure 11 for the DWM-Egmond model they seem not to agree with simulations with our DTU implementation of the DWM model, however with the uncertainty of just assuming a similar turbine operation but without knowing the details of the turbine
    - The authors are encouraged to share and upload more details of their simulations so that the results can be checked with an original implementation of the so-called DWM-Egmond model.
    - Further, it is proposed to show a figure with e.g. the mean velocity of the wake deficit or the mean velocity cubed (to show reduction in power of the downstream turbine) and otherwise in the same way as Figure 9. The mean velocity is a more robust characterization of the wake deficit than the minimum value velocity within the deficit. The minimum value can easily be influence by the details of the aerodynamic modelling of the turbine.

Response: A comparison between the static deficit, respectively the solution of the thin-shear layer equations with an implementation of the DTU has already been carried out. The model has been compared to the Python implementation of Jaime Yikon Liew. The two implementations match very well (see following figures). The figures show results from the so-called DWM-Egmond model of both model implementations and their difference (ε is the mean difference).

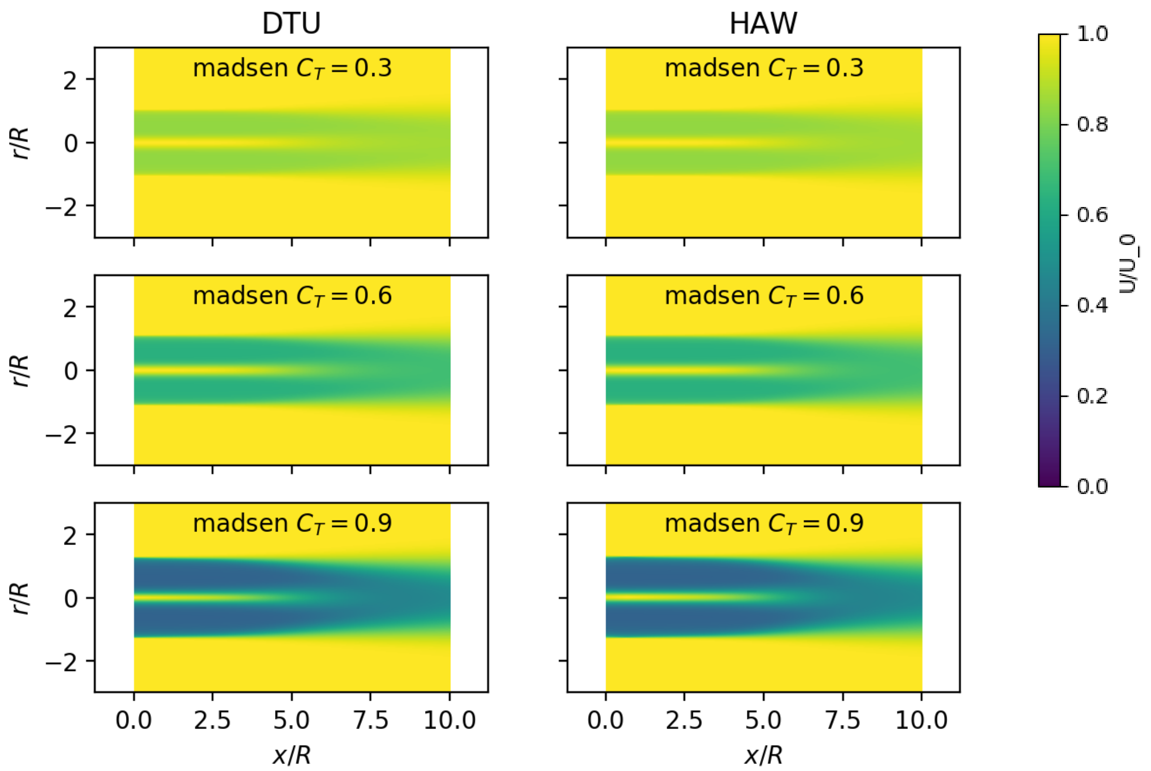

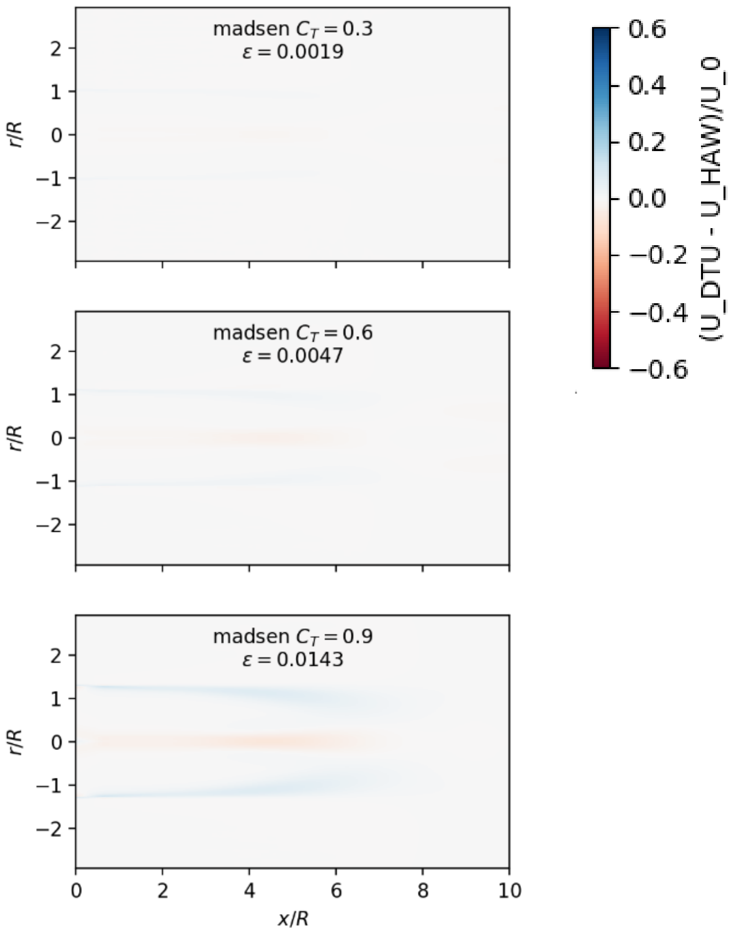

The comparison between the two implementations can be found here:
https://github.com/jaimeliew1/dwm_benchmark

The normalized mean wind speed for all turbulence intensity bins are illustrated in the following:

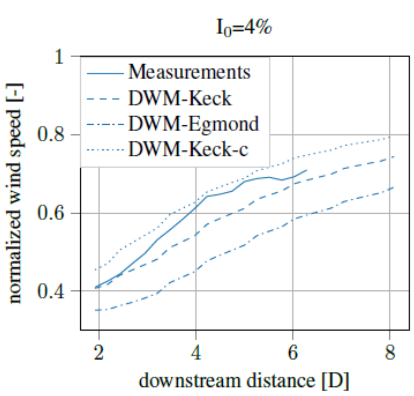

(a)

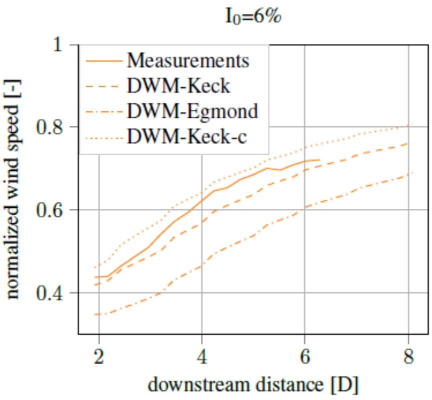

(b)

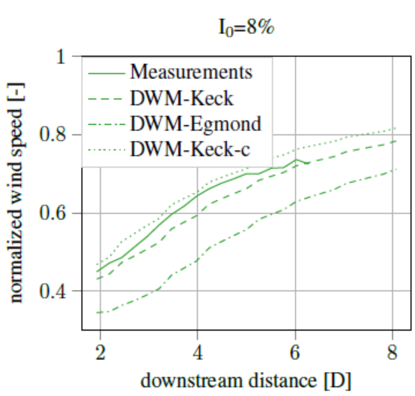

(c)

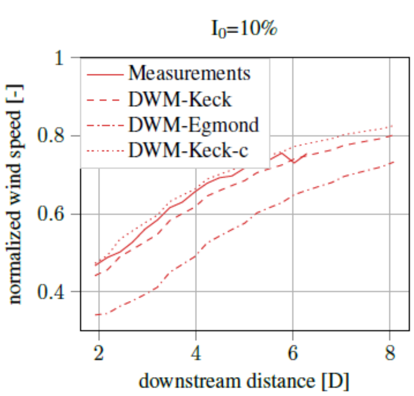

(d)

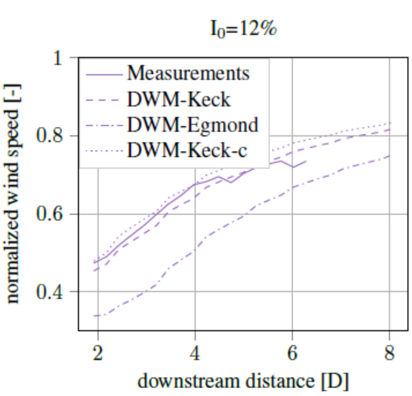

(e)

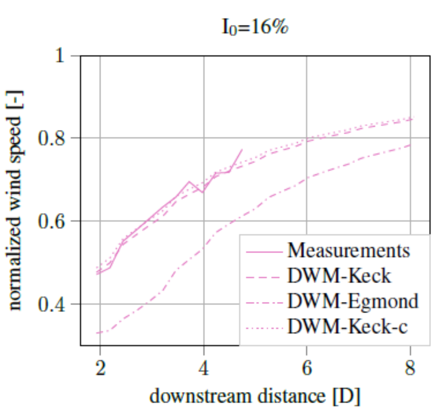

(f)

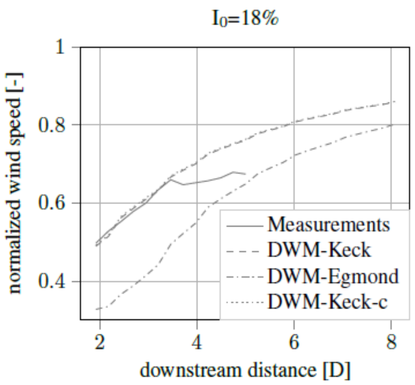

(g)

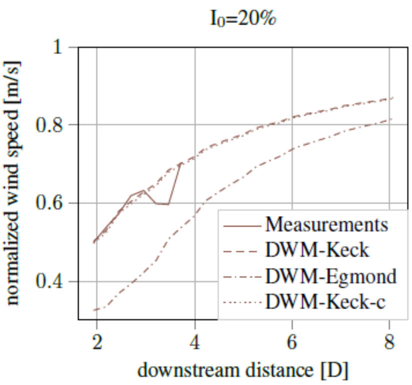

(h)

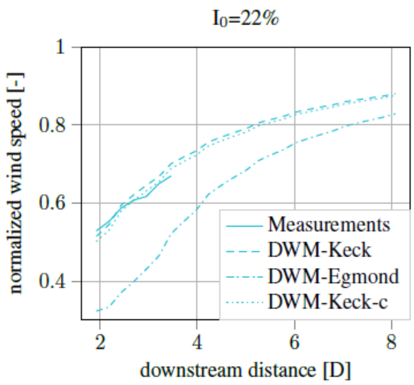

(i)

The mean wind speed over a distance of +/- 60m from the wake center is illustrated. Furthermore, a graph from the RMSE between these curves and all model versions is illustrated.

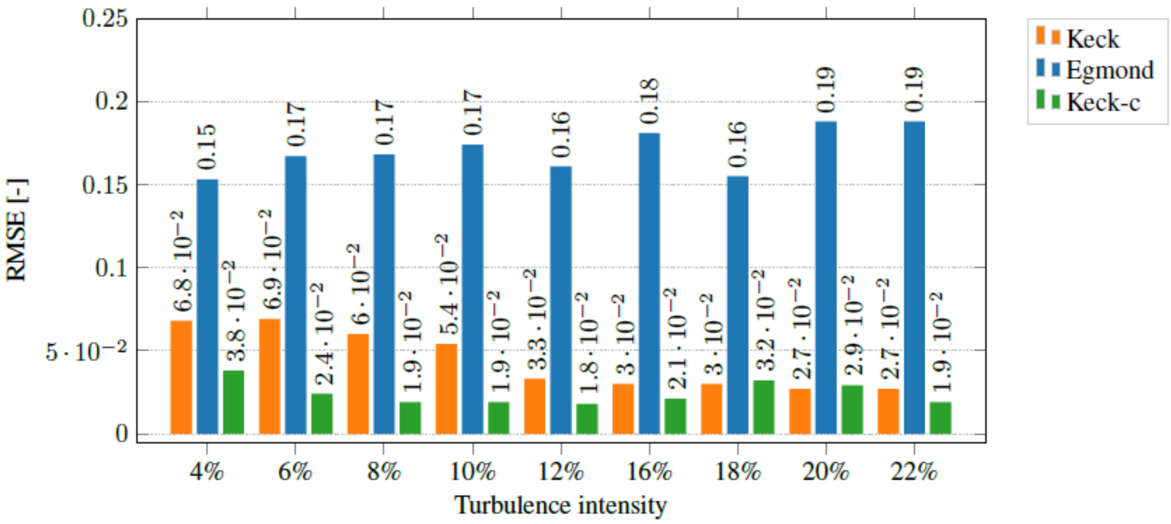

The improvement of the mean wind speed is less clear in comparison to the normalized minimum wind speed. But nevertheless, there is an improvement in almost all turbulence intensity bins or similar good results could be achieved. In the smaller turbulence intensity bins and closer distances, the recalibrated DWM-Keck-c model agrees less well with the measurements. At closer distances the wind speed deficit gets coarse since less scan points are gathered and the influence of the turbulence at the tails is much higher. This leads to an error in the mean wake wind speed but not in the minimum wind speed, which explains these discrepancies. This is the reason why the minimum wake wind speed is illustrated in the paper and used for the recalibration of the DWM-model.

Some final conclusive remarks

- There is no discussing of the impact of the findings. Changing the wake recovery characteristics have obviously an impact on power production and loads.
    - For the Egmond aan Zee case the DWM model was as mentioned calibrated to the power reduction of the second turbine in a row relative to the first one for different spacings and turbulence intensities. Using this calibration an overall good correlation of simulated and measured loads was found.
    - Have the present recalibrated model been used for power and load simulations and compared with measurements in the present wind farm?
    - The reviewer finds that due to the above mentioned uncertainties/limitations related to the measurements of the deficits in the meandering frame of reference there will be a bias of the measured deficits being more smooth. Please comment on this view.

Response: The comparison of the recalibrated model with power productions and loads in the wind farm is currently analyzed and will be published soon.
Comments according to the bias in measuring the wind speed deficit in the meandering frame of reference were answered directly at the specific positions above. A graph with DWM model simulations with and without vertical meandering was added.

List of the most relevant changes in the manuscript:

1. The title is adjusted to: DWM model calibration using nacelle mounted lidar systems.
2. A detailed description of the metmast measurement equipment has been added in written and visual form (Figure 2) in Section 2 “Wind farm”.
3. Section 3 “Data filtering and processing” has been restructured and a workflow was added to clarify the filtering procedure. A more detailed description of LiDAR specifications and sample frequencies is outlined.
4. A comparison of the simulated wind speed deficit with the DWM model in the complete MFR and without eliminating the vertical meandering in the wind speed deficit has been added with Figure 4.
5. To clarify that the vertical meandering is neither eliminated in the measurements nor in the simulations, the abbreviation HMFR (horizontal meandering frame of reference) is introduced and used instead of MFR.
6. A discussion regarding the uncertainties due to yaw misalignments and the determination of the ambient conditions is added in Sections 3 and 7.
7. To deliver a more quantitative comparison between the different DWM model versions and the measurements, a graph of the RMSE is added in Figure 14.
8. The language and argumentation have been adjusted, so that a more concise language is used throughout the manuscript.

~~Measuring dynamic wake characteristics with nacelle mounted LiDAR~~ DWM model calibration using nacelle-mounted lidar systems

Inga Reinwardt[1], Levin Schilling[1], Peter Dalhoff[1], Dirk Steudel[2], and Michael Breuer[3]

[1]Dep. Mechanical Engineering & Production, HAW Hamburg, Berliner Tor 21, D-20099 Hamburg, Germany
[2]Dep. Turbine Load Calculation, Nordex Energy GmbH, Langenhorner Chaussee 600, D-22419 Hamburg, Germany
[3]Dep. of Fluid Mechanics, Helmut-Schmidt University Hamburg, Holstenhofweg 85, D-22043 Hamburg, Germany

Correspondence: Inga Reinwardt (inga.reinwardt@haw-hamburg.de)

Abstract. Light Detection And Ranging (LiDAR) systems have gained a great importance in today's wake characteristic measurements. The aim of this measurement campaign is to track the wake meandering and in a further step to validate the wind speed deficit in the meandering frame of reference (MFR) and in the fixed frame of reference using ~~nacelle mounted~~ nacelle-mounted LiDAR measurements. ~~The measurement campaign has been prepared in detail by preliminary simulations mimicking the LiDAR behavior and corresponding wind field simulations.~~ Additionally, a comparison ~~between the~~ of the measured and the modelled wake degradation in the MFR ~~and the measured one could be~~ was conducted. The simulations were done with two different versions of the Dynamic Wake Meandering (DWM) model. These versions differ only in the description of the quasi-steady wake deficit. Based on the findings from the LiDAR measurements~~the formulation of the~~ , the impact of the ambient turbulence intensity on the eddy viscosity definition in the quasi-steady ~~wake deficit in the DWM model has been adjusted, so that the recalibrated model coincides very well with~~ deficit has been investigated and, subsequently, an improved correlation function has been determined, resulting in very good conformity between the new model and the measurements.

1 Introduction

Wake calculation of neighbouring wind turbines is a key aspect of every wind farm development. The aim is to estimate both, energy yield of the whole ~~windfarm~~ wind farm and loads on single turbines, as accurately as possible. One of the main models for calculating the wake-induced turbulence in a wind farm is the so-called Frandsen model (see, for example, Frandsen (2007)). Previous measurement campaigns have shown that this model delivers conservative results for small turbine distances ~~(Reinwardt et al. (2018) and Gerke et al. (2018))~~(Reinwardt et al., 2018; Gerke et al., 2018). This is particularly important for onshore wind farms in densely populated areas, where a high energy output per utilized area is crucial. In such cases, the usage of a more accurate description of the physical behaviour of the wake, as defined in the DWM model, seems appropriate. The DWM model is based on the assumption that the wake behaves as a passive tracer, which means, the wake itself is deflected in vertical and horizontal direction (Larsen et al., 2008b). The combination of this deflection and the shape of the wind speed deficit leads to an increased turbulence at a fixed position downstream. This plays an eminent role for the loads of a turbine located downstream of another turbine (Larsen et al., 2013). Therefore, a precise description of the meandering itself and the wind speed deficit in the meandering frame of reference (MFR) as well as a detailed validation of the wind speed deficit definition is fundamental.

LiDAR systems are highly suitable for wake validation purposes. Especially, the so-called scanning LiDAR systems ~~, which are capable of measuring a two-dimensional wind field,~~ offer great potential for detailed wake analysis. ~~With a scanning LiDAR device it is possible to detect the wake~~ These LiDARs are capable of scanning a three-dimensional wind field, so that the line of sight (LOS) wind speed can be measured subsequently at different positions in the wake, thus enabling the detection of the wake meandering as well as the shape of the wind speed deficit in the MFR. That is the reason why such a device is used in the measurement campaign outlined here. Several different measurement campaigns with ground based and ~~nacelle mounted~~ nacelle-mounted LiDAR systems have already been carried out in the last years, some of them even with the purpose of tracking wake meandering and validation of wake models.

In Bingöl et al. (2010) the horizontal meandering has been examined with a ~~nacelle installed~~ nacelle-installed continuous wave (CW) LiDAR. The campaign confirms the passive tracer assumption, which is essential for the definition of the meandering in the DWM model. Furthermore, the wind speed deficit in the MFR has been investigated for some distances. Due to the fact that the CW LiDAR can not measure simultaneously in different downstream distances, the beam has been focused successively to different downstream distances. In Trujillo et al. (2011) the analysis has been extended to a two-dimensional scan. The measured wind speed deficit in the MFR has been compared to the Ainslie wake model ~~(see Ainslie (1988))~~(Ainslie, 1988) , which constitutes the basis of the deficit's definition in the DWM model.

Additionally, in Machefaux et al. (2013) ~~,~~ a comparison of measured lateral wake meandering based on pulsed scanning LiDAR measurements has been presented. Special attention is paid to the advection velocity of the wake, which is estimated with measured and low-pass filtered wind directions at the metmast (based on the assumptions of the DWM model) and the wake displacement at certain downstream distances. The analysis shows that the advection velocity calculated by the N.O. Jensen model is in relatively good agreement. Finally, the study compares the measured expansion of the wake in the fixed frame of reference (FFR) to CFD simulations and simple analytical engineering models. The wake expansion calculated by simple analytical engineering models is well in line with LiDAR measurements and CFD simulations, but also depicts potential for further improvements, which is why a new empirical model for single-wake expansion is proposed in Machefaux et al. (2015). In Machefaux et al. (2016) a measurement campaign is presented, which involves three ~~nacelle mounted~~ nacelle-mounted CW scanning LiDAR devices. The investigation includes a spectral analysis of the wake meandering, a comparison of the measurements to the assumptions in the DWM model as well as a comparison of the wind speed deficit profile in a merged wake situation to CFD simulations.

It should be noted that the references listed here are only the most essential, on which the present measurement campaign builds up. Several campaigns including either LiDAR systems or meandering observations as well as wake model validations have been conducted in the past. The outlined analysis transfers some of the procedures of tracking the wake meandering to measurement results from an onshore wind farm with small turbine distances. Particular focus is put on the investigation of the wind speed deficit's shape in the MFR and the degradation of the wind speed deficit in downstream direction. The latter can be captured very well with the used ~~nacelle mounted~~ nacelle-mounted pulsed scanning LiDAR systems due to the fact that it measures simultaneously in different downstream distances. Thus, a detailed comparison of the predicted degradation of the wind speed deficit between the DWM model and the measurement results is possible. Furthermore, the collected LiDAR measurements are used to recalibrate the DWM model, which enables a more precise modeling of the wake degradation. As a consequence, the calculation of loads and energy yield of the wind farm can be improved.

~~In the following~~The remaining document is arranged as follows: In Section 2, the investigated wind farm and the installed measurement equipment are described in detail. Afterwards, in Section 3, an explanation of the data processing and filtering of the measurement results is given. ~~Furthermore, a~~ Sections 4, 5, and 6 focus on the description of the theoretical backround and a hands-on implementation of the DWM model is introduced. Based on the outlined measurement results, a recalibration of the defined degradation of the wind speed deficit in the DWM model is proposed in Section 6. A summary of the measurement results can be found in Section 7 and a comparison to the original DWM model as well as the recalibrated version is presented in ~~the last sections.~~ Section 8. Finally, all findings are concluded in Section 9.

2 Wind farm

The investigated onshore wind farm (Figure 1) located in the Southeast of Hamburg (Germany) consists of five closely spaced Nordex turbines (1x N117 3 MW and 4x N117 2.4 MW) ~~with small turbine distances and a~~ and an IEC compliant 120 m metmast, which is situated two rotor diameters ($D = 117\,\mathrm{m}$) ahead of the wind farm in the main wind direction (west-southwest). It is equipped with 11 anemometers, two of which are ultrasonic devices, three wind vanes, two temperature sensors, two thermohygrometers, and two barometers. The sensors are distributed along the whole metmast, but at least one of each is mounted in the upper eight meters (see Figure 2). The thrust as well as the power coefficient curves for both wind turbines are illusatretd in Figure 3. There are no other turbines in the immediate vicinity and the terrain is mostly flat. Only in further distances (more than 1 km) the terrain is slightly hilly (approx. 40 m). Two turbine nacelles are equipped with a pulsed scanning LiDAR system (Galion G4000). ~~Furthermore, three turbines are equipped with load measurements.~~ The wind farm layout with all ~~previously mentioned~~ installed measurement devices is shown in ~~Figure 1. The LiDAR system of WTG 1~~ Figure 1 (the displayed load measurements are not in the scope of this paper, but will be introduced in future publications). One LiDAR system is installed on top of the nacelle of WTG 2 (N117 2.4 MW), facing backwards. The second LiDAR system is installed inside the nacelle of WTG 1 (N117 3 MW) and measures through a hole in the rear wall. ~~The second LiDAR system is installed~~ In this case, mounting the device on top of the nacelle ~~of WTG 2, also facing backwards. Nacelle mounted~~ is not possible, as the area is occupied by a recuperator. The positions of both devices are displayed in Figure 2. Even though the setup reduces the field of vision, the measurement campaign described in this paper is not influenced by this restriction. On the plus side, the LiDAR system is not exposed to weather. Finally, nacelle-mounted differential GPS systems help tracking the nacelle's precise position as well as yaw movements with a centimeter range accuracy.

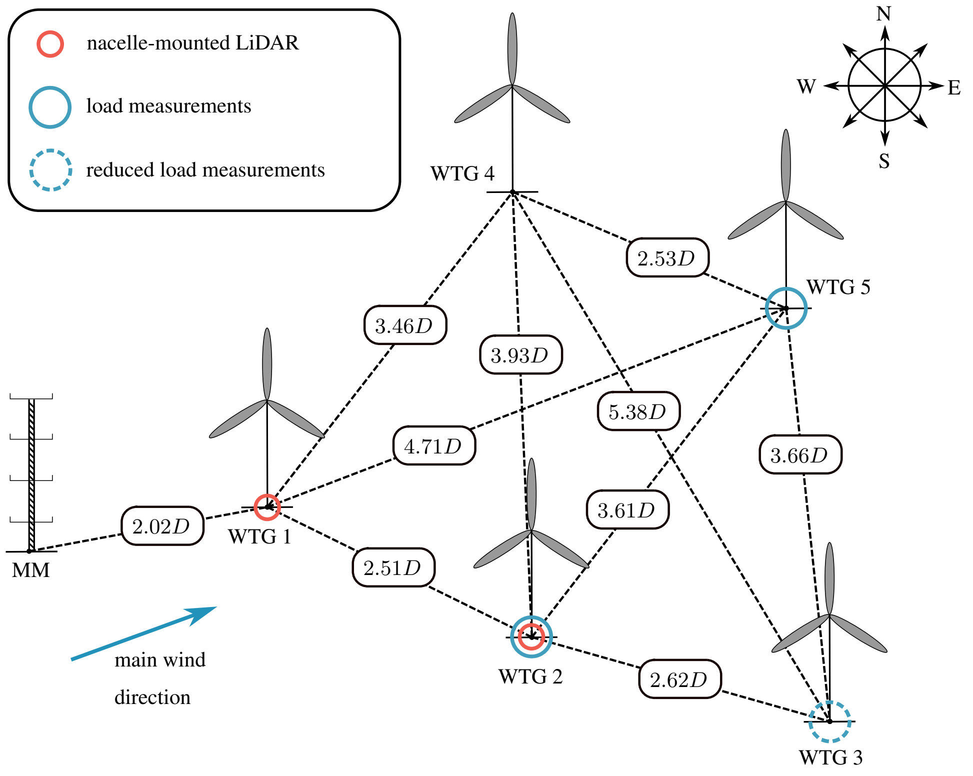

Figure 1. Wind farm layout with measurement equipment.

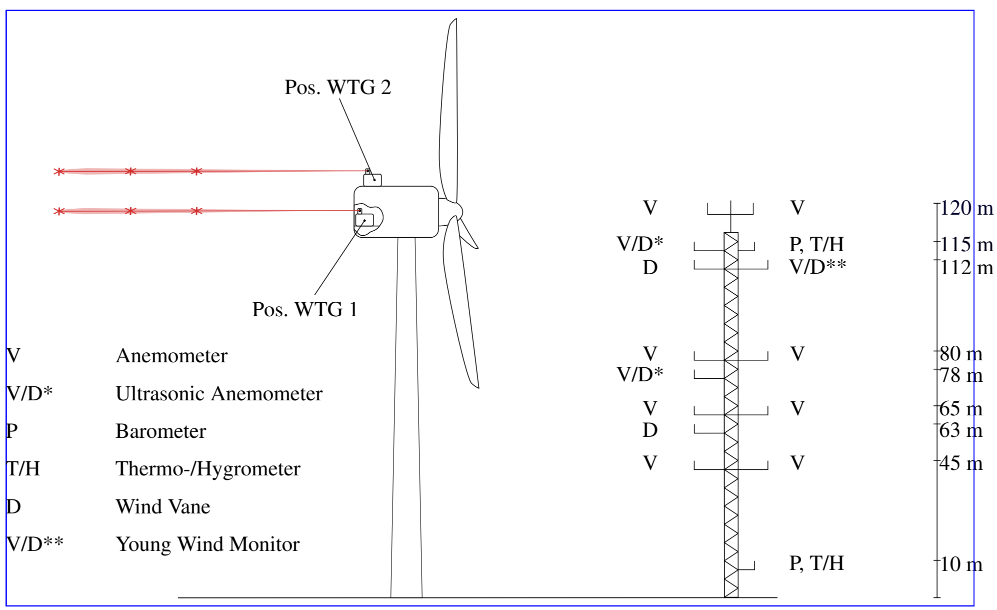

Figure 2. Metmast measurement equipment and LiDAR positions.

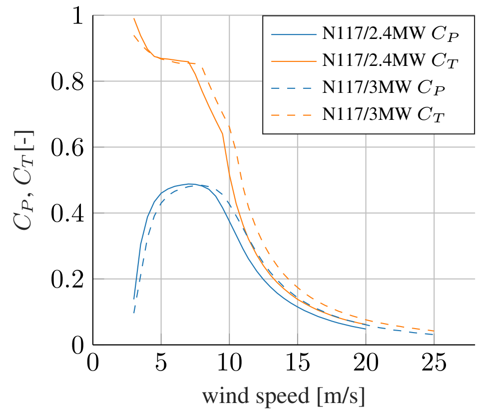

Figure 3. Power and thrust coefficients over wind speed for the N117/3MW and the N117/2.4MW turbines.

3 Data filtering and processing

~~The measured~~ The LiDAR data are filtered ~~and sorted~~ in accordance with ~~ambient wind speed, ambient turbulence intensity, wind shear, atmospheric stability, and wind direction. The ambient conditions are determined by the metmast~~the wind direction, so that ~~only measurement results with free inflow at the metmast are considered. Additionally, results~~ LiDAR data without free inflow of the wake generating turbine as well as LiDAR measurements in the induction zone of another turbine are rejected. This leads to the remaining wind direction sectors listed in Table 1. The remaining sectors are relatively small, especially for

Table 1. Considered wind direction sectors per wake generating turbine in the measurement campaign. Wind direction sectors without free inflow of the metmast and the turbine as well as measurements in the induction zone of another turbine are omitted.

	lower limit [°]	upper limit [°]
WTG 1	160	190
	320	350
WTG 2	150	160
	240	250

the LiDAR on WTG 2, which reduces the amount of usable measurement data drastically. ~~Atmospheric stability is determined by the gradient Richardson number, which is calculated with temperature and wind speed measurements at two different heights. A negative Richardson number implies unstable and a positive Richardson number stable atmospheric stratification.~~ Additionally, the measured LiDAR data are sorted into turbulence intensity bins for the further validation and recalibration of the DWM model. The ambient conditions are determined by 10-minute time series statistics from the metmast, hence only measurement results with free inflow at the metmast are useable. Only situations with normal power production of the wake generating turbine are considered. The turbine operation mode is identified through the turbine's Supervisory Control and

Data Acquisition (SCADA) system. The statistics of the 10-minute time series are applied to identify the operational mode. Furthermore, the data has been analyzed according to yaw misaligments, so that no data with turbine misalignments greater than 6° are considered in the analysis. The misalignment is determined by the GPS systems and the metmast wind direction. Moreover, the LiDAR data are ~~moreover~~ filtered by the power intensity of the measurement results, which is closely related to the signal-to-noise ratio (SNR) of the measurements. Results with an intensity lower than 1.01 have been discarded. The ~~range gate length~~ pulse repetition rate of the LiDAR system is ~~30 m. The~~ 15 kHz. The ray update rate is about 1 Hz (depending on the atmospheric conditions), so it averages over approximately 15000 pulses. The sample frequency is 100 MHz. Considering the speed of light, this delivers a point length of 1.5 m. The range gate length is 30 m, hence 20 points are used per range gate. The measurement time increases with the number of range gates~~due the fact that the~~, because the internal data processing time increases. Thus, to decrease the measurement time, the number of range gates has been limited, so that the farthest scan point is ~~750 m~~ 750 m downstream. Additionally, the scanning time of each complete horizontal line scan is verified by the timestamp of each scan to ensure that the meandering can really be captured. In summary, this leads to the following filtering procedure for the measured LiDAR data:

1. Filtering according to the wind direction determined by the metmast (free inflow at metmast and wind turbine and no induction zone from other turbines)
2. Filtering according to the normal power production determined by the turbine's SCADA system
3. Filtering according to yaw misaligment
4. Filtering according to the SNR of the LiDAR measurements
5. Filtering according to scan time
6. Grouping all data sets in turbulence intensity bins with a bin width of 2 %

LiDAR systems measure the line of sight ~~(LOS)~~ velocity. The wind speed in downstream direction is then calculated from the LiDAR's LOS velocity and the geometric dependency of the position of the laser beam relative to the main flow direction as outlined in Machefaux et al. (2012). Thus, the horizontal wind speed is defined as

$$U(t) = U_{LOS} \cdot \frac{1}{\cos(\theta) \cdot \cos(\phi)} \,, \tag{1}$$

where θ is the azimuth angle and ϕ the elevation angle of the LiDAR scan head. This seems to be a suitable approach for small scan opening angles ~~as~~ like in the measurement campaign presented here. ~~Thus, the horizontal wind speed is defined as:~~

$$U(t) = U_{LOS} \cdot \frac{1}{\cos(\theta) \cdot \cos(\phi)}$$

~~with θ being the azimuth angle and ϕ the elevation angleof the LiDAR scan head~~The biggest opening angle in the scan pattern is 20°. Nevertheless, if there is yaw misalignment, this could have an impact on the overall results. To decrease the uncertainties based on yaw misalignments, the measurement data has accordingly been filtered. The yaw misalignment has the biggest impact at the largest scan opening angle, i.e., a misalignment of 6° at an opening angle of 20° leads to an overestimation of the wind speed of less than 5 %.

4 Wind speed deficit in ~~MFR~~ HMFR calculation

The meandering time series and the wake's horizontal displacement are determined with the help of a Gaussian fit. Trujillo et al. (2011) assume that the probability of the wake position in vertical and horizontal direction is completely uncorrelated, so that the two-dimensional fitting function can be expressed as follows:

$$f_{2D} = \frac{A_{2D}}{2\pi\sigma_y\sigma_z}\exp\left[-\frac{1}{2}\left(\frac{(y_i-\mu_y)^2}{\sigma_y^2}+\frac{(z_i-\mu_z)^2}{\sigma_z^2}\right)\right], \tag{2}$$

~~with~~ where σ_y and σ_z ~~being~~ are the standard deviations of the horizontal and vertical displacements μ_y and μ_z, respectively. In the analysis presented here, only results from a horizontal line scan are analyzed, so that no vertical meandering is ~~considered and the~~ eliminated from the wind speed deficit and the deficit's depth is less pronounced in comparison to the real MFR. To clarify that the vertical meandering is not eliminated in the present investigation, but included in the wind speed deficit, the abbreviation HMFR (horizontal meandering frame of reference) is introduced and henceforth used instead of MFR. A comparison of the wind speed deficit simulated with the DWM model in the complete MFR and the HMFR is illustrated in Figure 4. The simulations were carried out for a small downstream distance of $2.5D$ and a high turbulence intensity of 16 %. There are only small discrepancies around the center of the wake, which validates the present assumption.

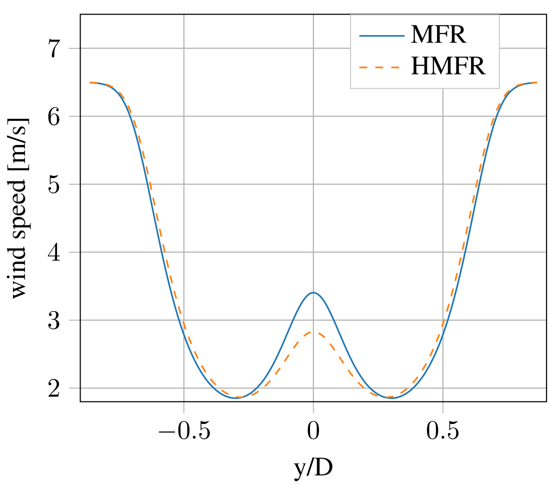

Figure 4. Wind speed deficit at a downstream distance of $2.5D$ and an ambient turbulence intensity of 16 %.

Since the vertical meandering is neglected, the measurement results are fitted to a one-dimensional Gaussian curve defined as follows:

$$f_{1D} = \frac{A_{1D}}{\sqrt{2\pi}\sigma_y} \exp\left(-\frac{1}{2}\frac{(y_i - \mu_y)^2}{\sigma_y^2}\right) , \tag{3}$$

where A_{1D} represents a scaling parameter. The measured wind speeds are fitted to the Gauss shape via a least-squares method. Thereby, only fitted horizontal displacements μ_y that are ~~in~~ between -200 m and 200 m are used for further validations of the mean wind speed in the ~~MFR~~HMFR. A horizontal displacement of more than 200 m cannot be represented by the Gauss fit due to a lack of measurement points. However, such an event is highly improbable (e.g., the DWM model predicts the wind speed deficit's probability at the horizontal position of 200 m to be $2 \cdot 10^{-22}$ for an ambient wind speed of 6.5 m/s and an ambient turbulence intensity of 8 %). ~~Generally, this method of finding the wake position has proved to be very robust during the whole measurement campaign.~~

The entire method of calculating the wind speed deficit in the ~~MFR~~ HMFR is illustrated in Figure 5 and can be described as follows: The LiDAR system takes measurements from the nacelle of the turbine in downstream direction, which deliver the

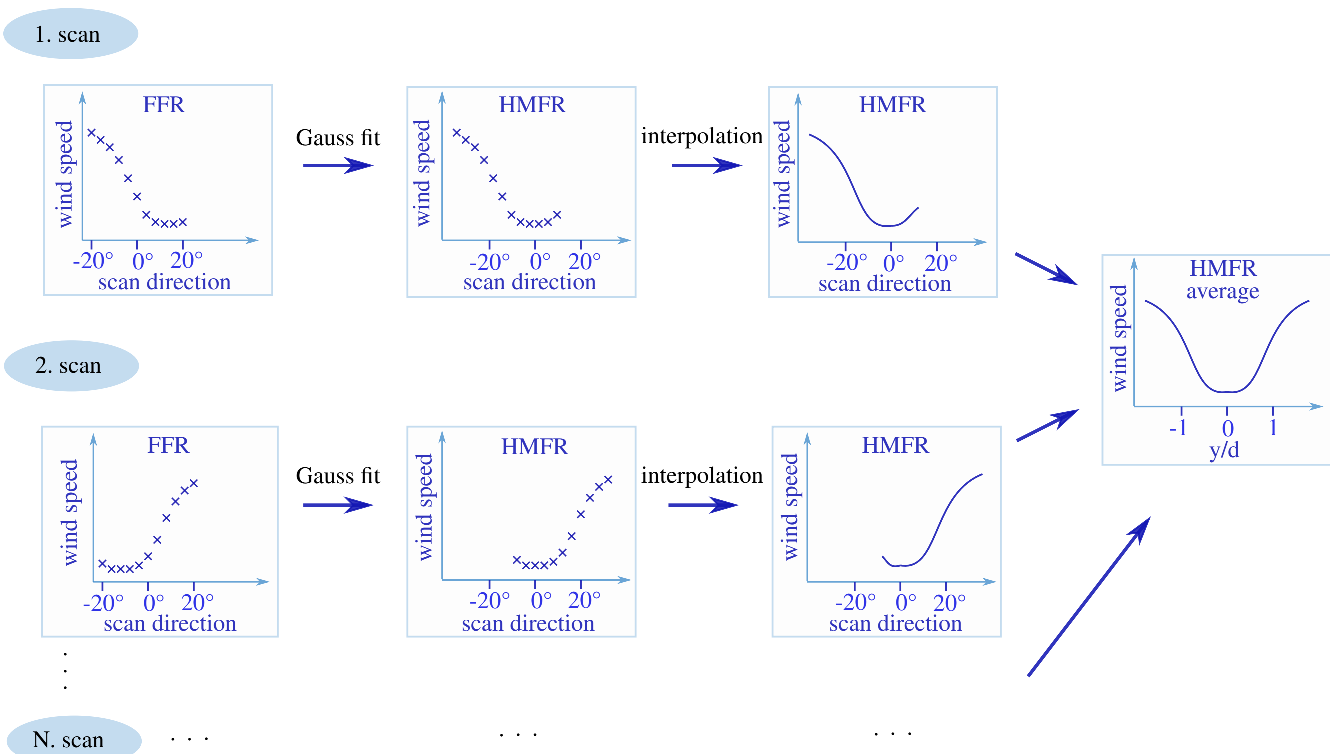

Figure 5. Method for the determination of the mean wind speed deficit in the ~~MFR~~HMFR.

wind speed deficit in the nacelle frame of reference or even in the FFR (see left side of Figure 5) if the turbine is not moving (this ~~can be~~ is ensured by the GPS systems). A Gauss curve is then fitted into the scanned points as explained previously. It provides the horizontal displacement of the wake, so that each scan point can be transferred into the ~~MFR~~ HMFR with the calculated displacement (see middle diagrams in Figure 5). The last step illustrated in the diagrams is the interpolation to a regular grid. These three steps are repeated for a certain number of scans N (e.g., approx. 37 for a 10-min time series). Finally, the mean value of all single measurement results in the ~~MFR~~ HMFR is calculated. It should be noted that it is mandatory to interpolate to a regular grid. Otherwise it would not be possible to take the mean of all scans since the horizontal displacement differs at each instant ~~in~~ of time and, thereupon, the measurement points are transmitted to a different location in the ~~MFR~~HMFR. After averaging, the plausibility of the results is inspected. If the calculated minimum mean wind speed in the ~~MFR~~ HMFR is higher than the minimum mean wind speed in the FFR, it is assumed that the Gauss fit failed and the results are no longer considered. In theory, the wind speed deficit in the HMFR should be more pronounced than the measured one in the FFR, wherefore this fundamental plausibilty check is added.

5 LiDAR simulation

One of the most challenging parts of this specific measurement campaign is the low ray update rate of the LiDAR system, which is considerably smaller than in the previously introduced measurement campaigns ~~(see Bingöl et al. (2010) and Trujillo et al. (2011)). The issue is compensated by an optimized scan pattern determined by~~ (Bingöl et al., 2010; Trujillo et al., 2011) . To ensure that the meandering as well as the wind speed deficit in the HMFR can be captured with the devices used, LiDAR and wind field simulations have been conducted in advance. The simulations incorporate LiDAR specifications (e.g., beam update rate and scan head angular velocity) and wind farm site conditions (ambient turbulence intensity and wind shear). The ~~simulated~~ simulations assume perfect LiDAR measurements, where no probe volume averaging is considered and the LiDAR measures the horizontal wind speed directly. The wind field is simulated at halfway of the range gate. The simulated LiDAR "takes measurements" in a simulated wind field that is generated by the DWM model and includes wake effects as well as ambient turbulences. A detailed description of the model is given in Section 6. The in-house code is written in Python. From these "measured" wind speeds the meandering is determined via Gaussian fits as previously explained and implemented in the real measurement campaign. Simulations are performed for different scan patterns, ambient conditions, and downstream distances to ~~find an optimal~~ test the scan pattern, which for this one-dimensional scan consists of only 11 scan points scanned in a horizontal line from ~~to in steps.~~

~~In addition to the determination of the position of the wind speed deficit, the shape of the wind speed deficit in the MFR has also been estimated.~~ $-20°$ to $20°$ in $4°$ steps. The "measurement" results of the simulated meandering time series are shown in Figure 6(a), whereas the corresponding wind speed deficit in the ~~MFR~~ HMFR is presented in Figure 6(b). The results are compared to the original meandering time series and the simulated wind speed deficit. The "measured" wind speed deficit in the simulated environment reproduces the simulated wind speed and its underlying meandering time series very well (the coefficient of determination R^2 is approximately 0.93). Although only 11 scan points are used for these plots, the curve of the wind speed deficit is very smooth. The reason for this behavior is the previously mentioned interpolation process. The distribution generated by the meandering process provides many scan points around the center of the wind speed deficit

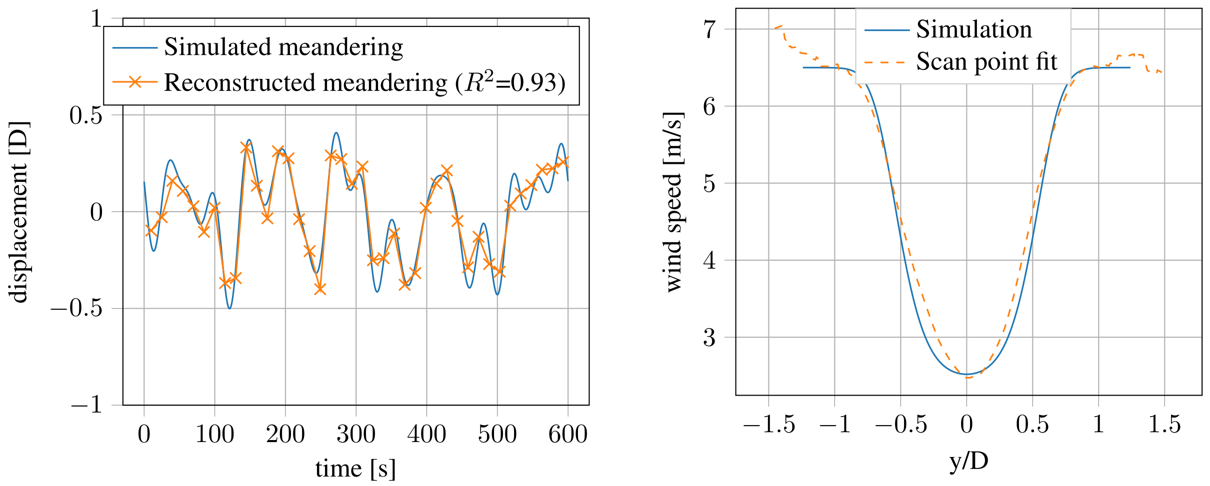

(a) (b)

Figure 6. Simulated and simulated “measured” meandering time series ~~(a)~~ **(a)** and wind speed deficit in the ~~MFR (b)~~ HMFR **(b)** at an ambient wind speed of 6.5 m/s.

and only a few at the tails. Therefore, the influence of turbulence at the tails is much higher, leading to a somewhat coarse distribution at the boundaries of the deficit. It should also be noted that since this is a one-dimensional scan, the simulated LiDAR “measures” the wind speed deficit only horizontally neglecting the wake’s less dominant vertical movement. Whenever the wind speed deficit in the HMFR is mentioned in subsequent validations, it implies the neglection of eliminating the vertical meandering from the wind speed deficit, which has only a marginal impact on the shape of the wind speed deficit in the ~~FFR~~real MFR (see Figure 4).

The LiDAR simulations indicate that the Gauss fit works more ~~reliable~~ reliably under optimal operating conditions, i.e., at optimal tip speed ratio, when the wind speed deficit is most pronounced and the power coefficient C_p has its maximum (see Figure 3). For the turbines examined, this applies ~~in~~ to a range of 5 m/s up to 8 m/s, so that only measurement results with ambient wind speeds in this interval are analyzed.

6 Dynamic wake meandering model

The measured wind speed deficit in the ~~MFR~~ HMFR is consecutively compared to the DWM model, which is based on the assumption that the wake behaves as a passive tracer in the turbulent wind field. Consequently, the movement of the passive structure, i.e., the wake deficit, is driven by large turbulence scales ~~(Larsen et al. (2007) and Larsen et al. (2008b))~~(Larsen et al., 2007, 2008b). The main components of the model are summarized in Figure 7(a). The model was built in-house and independent from any commercial software in Python.

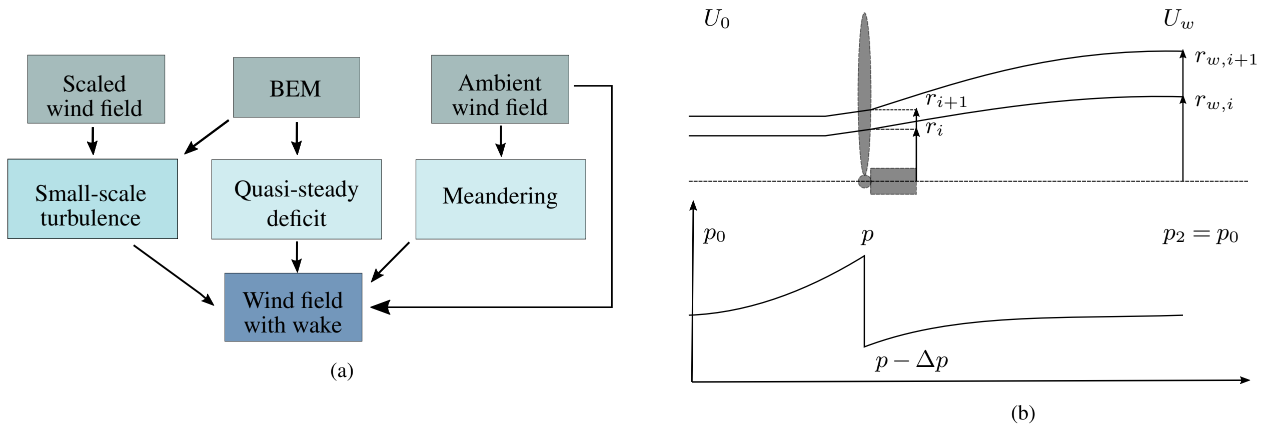

Figure 7. Components of the DWM model ~~(a)~~ **(a)** (Reinwardt et al., 2018) and schematic illustration of the wake expansion in the DWM model ~~(b)~~ **(b)** according to Madsen et al. (2010).

6.1 Quasi-steady wake deficit

One key point of the model is the quasi-steady wake deficit or rather the wind speed deficit in the MFR. ~~It compares directly to the LiDAR measurements after transforming the measurements into the MFR as explained in the last section.~~ In this study, two calculation methods for the quasi-steady wake deficit are compared with the LiDAR measurement results. A similar comparison of these models to metmast measurements in the FFR was published in Reinwardt et al. (2018). The quasi-steady wake deficit is defined in the MFR and consists of a formulation of the initial deficit emitted by the wake generating turbine and the expansion of the deficit downstream (Larsen et al., 2008a). The latter is calculated with the thin ~~shear-layer~~ shear layer approximation of the Navier-Stokes equations in ~~its~~ their axisymmetric form. This method is strongly related to the work of Ainslie (1988) and outlined in Larsen et al. (2007). The thin ~~shear-layer~~ shear layer equations expressed by the wind speed in axial and radial direction U and V_r, respectively, are defined ~~as follows:~~ by

$$U\frac{\partial U}{\partial x} + V_r\frac{\partial U}{\partial r} = \frac{1}{r}\frac{\partial}{\partial r}\left(\nu_T r\frac{\partial U}{\partial r}\right) \tag{4}$$

and

$$\frac{1}{r}\frac{\partial}{\partial r}(rV_r) + \frac{\partial U}{\partial x} = 0. \tag{5}$$

The first part of the quasi-steady wake deficit, the initial deficit, serves as a boundary condition when solving the equations. In both methods used to determine the quasi-steady wake deficit, the initial deficit is based on the axial induction factor derived from the blade element momentum (BEM) theory. Pressure terms in the thin ~~shear-layer~~ shear layer equations are neglected. The error that inherently comes with this assumption is accommodated by using the wind speed deficit two rotor diameters downstream (beginning of the far-wake area) as a boundary condition for the solution of the thin ~~shear-layer~~ shear layer equations. The equations are solved directly from the rotor plane by a finite-differences method with a discretization in axial and radial direction of $0.2D$ and $0.0125D$ combined with an eddy viscosity (ν_T) closure approach. The two methods that are compared with the LiDAR measurements only differ in the definition of the initial deficit and the eddy viscosity formulation.

6.1.1 DWM-Egmond

For the first method the following formulae are given to calculate the initial deficit. Hence, the boundary condition for solving the thin ~~shear-layer~~ shear layer equations are (Madsen et al., 2010):

$$U_w\left(\frac{r_{w,i+1}+r_{w,i}}{2}\right)=U_0(1-2a_i) \tag{6}$$

and

$$r_{w,i+1}=\sqrt{\frac{1-a_i}{1-2a_i}\left(r_{i+1}^2-r_i^2\right)+r_{w,i}^2}\,f_w \tag{7}$$

with

$$f_w=1-0.45\bar{a}^2\ , \tag{8}$$

where $\bar{a}$ represents the mean induction factor along all radial positions i, r_i the rotor radius and $r_{w,i}$ the wake radius. The boundary condition of the radial velocity component is $V_r=0$. The initial wake expansion and the corresponding radial positions as well as the pressure recovery in downstream direction are illustrated in Figure 7(b). The eddy viscosity ν_T used in ~~equation~~ Equation (4), is calculated in this first approach as follows (Larsen et al., 2013):

$$\frac{\nu_T}{U_0R}=k_1F_1(\tilde{x})F_{amb}(\tilde{x})I_0+k_2F_2(\tilde{x})\frac{R_w(\tilde{x})}{R}\left(1-\frac{U_{min}(\tilde{x})}{U_0}\right) \tag{9}$$

with $k_1=0.1$ and $k_2=0.008$. The eddy viscosity is normalized by the ambient wind speed U_0 and the rotor radius R. The outlined definition consists of two terms. The first is related to the ambient turbulence intensity I_0, whereas the second depends on the shape of the wind speed deficit itself. The single terms are weighted with the factors k_1 and k_2. The filter functions F_1 and F_2 in ~~equation~~ Equation (9) depending on $\tilde{x}$ (downstream distance normalized by the rotor radius) are defined by IEC 61400-1 Ed.4 as follows:

$$F_1(\tilde{x})=\begin{cases}\left(\frac{\tilde{x}}{8}\right)^{3/2}-\frac{\sin\left(\frac{2\pi\tilde{x}^{3/2}}{8^{3/2}}\right)}{2\pi} & \text{for } 0\leq\tilde{x}<8\\ 1 & \text{for } \tilde{x}\geq 8\end{cases} \tag{10}$$

and

$$F_2(\tilde{x})=\begin{cases}0.0625 & \text{for } 0\leq\tilde{x}<4\\ 0.025\tilde{x}-0.0375 & \text{for } 4\leq\tilde{x}<12\\ 0.00105(\tilde{x}-12)^3+0.025\tilde{x}-0.0375 & \text{for } 12\leq\tilde{x}<20\\ 1 & \text{for } \tilde{x}\geq 20\ .\end{cases} \tag{11}$$

The filter function F_2 covers the lack of equilibrium between the velocity field and the rising turbulence in the beginning of the wake. F_1 is introduced to include the fact that the depth of the wind speed deficit increases in the near-wake area up to ~~(2...3)D~~ $(2\ldots3)D$ downstream of the turbine until it attenuates again in downstream direction (Madsen et al., 2010). The filter function as well as Equation (8) are calibrated against actuator disc simulations at a downstream distance of $2D$, the beginning of the far-wake area, where the wake is fully expanded (Madsen et al., 2010). A more detailed explanation of the nonlinear coupling function F_{amb} is given in Section 6.3. This calculation method (~~equations~~ Equations (6) to (11)) is subsequently named "DWM-Egmond" after the site, which is used for the calibration of the eddy viscosity in Larsen et al. (2013).

6.1.2 DWM-Keck

The second investigated method defines the initial deficit by the following equations (Keck, 2013):

$$U_w(r_{w,i}) = U_0\left(1-(1+f_u)\,a_i\right) \tag{12}$$

and

$$r_{w,i} = r_i\sqrt{\frac{1-\bar{a}}{1-(1+f_R)\,\bar{a}}} \tag{13}$$

with $f_u = 1.1$ and $f_R = 0.98$. The boundary condition of the radial velocity component is again $V_r = 0$. In Keck (2013) the final and recommended version of the model developed for the eddy viscosity is defined as follows:

$$\nu_T = k_1 F_1(\tilde{x})\; u^*_{ABL;\lambda<2D}\; l^*_{ABL;\lambda<2D} + k_2 F_2(\tilde{x}) \max\left(l^{*2}\left|\frac{\partial U(\tilde{x})}{\partial r}\right|, l^*\left(1-U_{min}(\tilde{x})\right)\right) \tag{14}$$

with $k_1 = 0.578$ and $k_2 = 0.0178$ and the filter functions:

$$F_1 = \begin{cases} \frac{\tilde{x}}{4} & \text{for } \tilde{x} < 4 \\ 1 & \text{for } \tilde{x} \geq 4 \end{cases} \tag{15}$$

and

$$F_2 = \begin{cases} 0.035 & \text{for } \tilde{x} < 4 \\ 1-0.965e^{-0.35(\tilde{x}/2-2)} & \text{for } \tilde{x} \geq 4 \end{cases}\;. \tag{16}$$

In contrast to the previously mentioned model (DWM-Egmond) atmospheric stability is considered in this final model description. Equation (14) involves the velocity $u^*_{ABL;\lambda<2D}$ and length scale $l^*_{ABL;\lambda<2D}$ fractions of the ambient turbulence, which is related to the wake deficit evolution (eddies smaller than ~~2D~~ $2D$). The velocity scale $u^*_{ABL;\lambda<2D}$ is besides the ambient turbulence intensity I_0 related to the ratio of the Reynolds stresses (normal stress in flow direction and the shear stress), which in turn are functions of the atmospheric stability. A detailed description of a method to introduce atmospheric stability in the DWM model can be found in Keck et al. (2014) and Keck (2013). In contrast to the final and recommended model in Keck (2013), atmospheric stability is not considered in this study, so that a previous model in Keck (2013) without consideration of atmospheric stability is used and the numerical constants k_1 and k_2 in ~~equation~~ Equation (17) are changed with respect to the first least-squares recalibration in Keck (2013). Furthermore, according to Keck (2013) it can be assumed that the mixing length l^* is equal to half of the wake width. This results in the following formulation of the eddy viscosity:

$$\frac{\nu_T}{U_0 R} = k_1 F_1(\tilde{x}) I_0 + k_2 F_2(\tilde{x}) \max\left(\frac{R_w(\tilde{x})^2}{R U_0}\left|\frac{\partial U(\tilde{x})}{\partial r}\right|, \frac{R_w(\tilde{x})}{R}\left(1 - \frac{U_{min}(\tilde{x})}{U_0}\right)\right) \tag{17}$$

with $k_1 = 0.0914$ and $k_2 = 0.0216$.

6.2 Meandering of the wake

The meandering of the wind speed deficit is calculated from the large turbulence scales of the ambient turbulent wind field. Thus, the vertical and horizontal movements are calculated from an ideal low-pass filtered ambient wind field. The cut-off frequency of the low-pass filter is specified by the ambient wind speed and the rotor radius as (Larsen et al., 2013):

$$f_c = \frac{U_0}{4R}. \tag{18}$$

The horizontal $y(t)$ and vertical $z(t)$ positions of the wind speed deficit are calculated based on the low-pass filtered ~~velocoties~~ velocities in horizontal and vertical directions according to the relations (Larsen et al., 2007):

$$\frac{\mathrm{d}y(t)}{\mathrm{d}t} = v(t) \tag{19}$$

and

$$\frac{\mathrm{d}z(t)}{\mathrm{d}t} = w(t), \tag{20}$$

where $v(t)$ and $w(t)$ are the fluctuating wind speeds at hub height. The ambient wind field, which is later on low-pass filtered, is generated in this work by a Kaimal spectrum and a coherence function (e.g., Veers, 1988). The temporal resolution of the generated wind field is 0.07 s.

6.3 ~~Small-scale turbulence~~

~~Another aspect of the DWM model is the definition of the small-scale turbulence generated through the wake shear itself as well as blade tip and root vortices. This part of the turbulence is calculated with a scaled homogeneous turbulent wind field also generated by a Kaimal spectrum. The scaling factor~~ $\cancel{k_{aw}}$ ~~is defined by (IEC 61400-1 Ed.4):~~

$$\cancel{k_{aw}(\tilde{x},\tilde{r}) = 0.6\left|1 - \tilde{U}(\tilde{x},\tilde{r})\right| + 0.35\left|\frac{\partial \tilde{U}(\tilde{x},\tilde{r})}{\partial \tilde{r}}\right|}$$

~~Equation uses the normalized wind speed deficit~~ $\cancel{\tilde{U}(\tilde{x},\tilde{r})}$ ~~based on the calculation of the initial deficit, which itself builds on the BEM theory and the aerodynamics of the turbine. This study analyzes only the mean wind speed in the MFR and the meandering itself. Therefore, the analysis of the small-scale turbulence is not part of the validation. Nevertheless, for the sake of completeness of the model is mentioned at this point.~~

6.3 Recalibration of the DWM model

The wind speed deficit measured by the LiDAR systems is used to recalibrate the wake degradation downstream or to be more precise the eddy viscosity description. In Larsen et al. (2013) a recalibration was already achieved by introducing a nonlinear coupling function F_{amb} into the ambient turbulence intensity term of the eddy viscosity definition (see ~~equation~~ Equation (9)). Furthermore, a comparison between the measured and simulated power based on the DWM model was carried out. It shows that the wind speed deficit degradation is too low for lower turbulence intensities and moderate to high turbine distances ~~the wind speed deficit degradation is too low~~in the model version from Madsen et al. (2010). For this reason~~the function~~ , the downstream distance dependent function F_{amb} ~~depending on the downstream distance~~ was introduced into the eddy viscosity description in Larsen et al. (2013).

A similar behavior but even more pronounced can be seen in the results in Section 7. Following the approach of Larsen et al. (2013), a function based on a least-squares calibration with the acquired LiDAR measurements is developed. This function is incorporated into the normalized eddy viscosity description in ~~eq~~Eq. (17), whereby it changes to:

$$\frac{\nu_T}{U_0 R} = k_1 F_{amb}(\tilde{x}) F_1(\tilde{x}) I_0 + k_2 F_2(\tilde{x}) \max\left(\frac{R_w(\tilde{x})^2}{R U_0}\left|\frac{\partial U(\tilde{x})}{\partial r}\right|, \frac{R_w(\tilde{x})}{R}\left(1 - \frac{U_{min}(\tilde{x})}{U_0}\right)\right) \tag{21}$$

with the constants $k_1 = 0.0924$ and $k_2 = 0.0216$ and the coupling function

$$F_{amb}(\tilde{x}) = a\tilde{x}^{-b} \tag{22}$$

with $a = 0.285$ and $b = 0.742$. The parameters a and b are the results of the least-squares calibration. It should be noted that the constant k_1 was also slightly adjusted by the recalibration, in which the normalized eddy viscosity definition of Keck (2013) has been used. ~~The reason for that is that~~ This derives from the fact that this model is already in ~~relatively~~ good agreement with the measurement results in most turbulence intensity bins as demonstrated in Section 8 and also in Reinwardt et al. (2018).

7 Measurement results

The measurement campaign lasted from January to July 2019. Both LiDAR systems, introduced in Section 2, were used to collect the data. Results of the meandering time series over 10 minutes are exemplarily shown in Figure 8(a). The maximum displacement of the wake is about ~~0.5D~~$0.5D$, which is equivalent to 58.5 m. The results are derived from a 10-min time series with an ambient wind speed of 6.44 m/s and an ambient turbulence intensity of 11.7 %. Some of the metmast detected ambient conditions (wind speed U_0, turbulence intensity I_0, wind shear α and wind direction θ) are given in the title of the figure. The corresponding mean wind speed deficit is illustrated in Figure 8(b). The wind speed decreases to less than 3 m/s in full wake situations. As explained in Section 5, the tails of the curve are relatively coarse since less scan points were gathered. It can also be seen that the ambient wind speed is not even reached at the edges of the curve. The opening angle of the scan appears too small to capture the whole wake at this distance. Towards the left part of the wind speed deficit (at negative y distances) a bigger part of the wake is captured. This arises from the fact that the horizontal displacement is more often positive than negative and, therefore, more measurement results are collected towards the left part of the wind speed deficit curve.

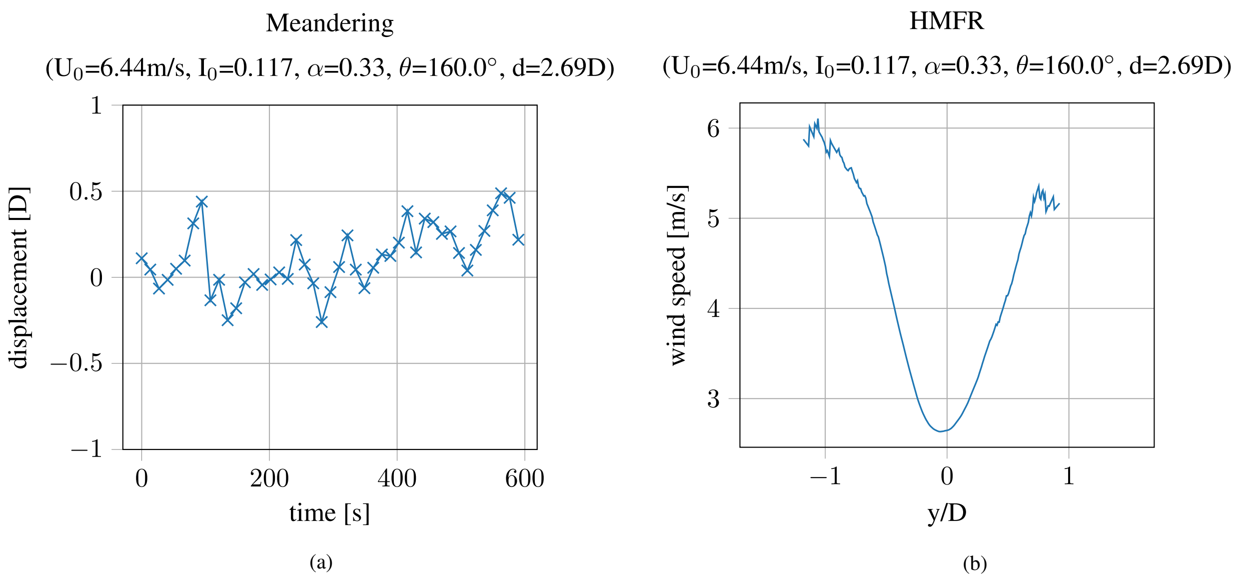

Figure 8. Meandering time series **(a)** and wind speed deficit in the ~~MFR~~ HMFR **(b)** at ~~2.69D~~ 2.69D downstream of the turbine.

The used LiDAR system is capable of measuring several range gates simultaneously in 30 m intervals. The results of all detected range gates for the data set presented in Figure 8 are shown in Figure 9(a). The closest distance is ~~1.92D~~

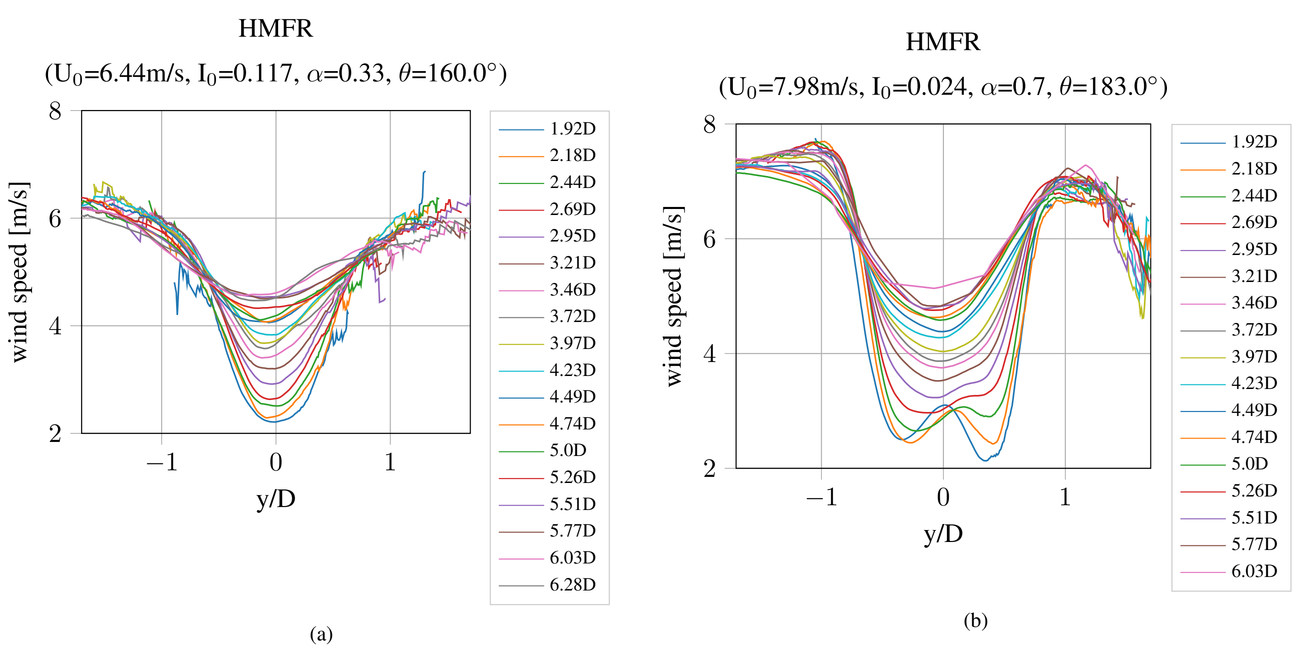

Figure 9. Wind speed deficit in ~~MFR~~ the HMFR for an ambient turbulence intensity of 11.7 % **(a)** and a turbulence intensity of 2.4 % **(b)**.

$1.92D$ downstream and the farthest is ~~6.28D~~ $6.28D$. The degradation of the wind speed deficit in downstream direction is clearly identifiable. As for the single distance case (Figure 8), for most range gates a bigger database is captured at the left part of the wind speed deficit, resulting in smoother curves. The presumption of a too small opening angle of the scan, as stated before, proves true. With increasing downstream distances the captured wind speed deficits get closer to integrity. A broader scan angle would result in more detailed wind speed deficits for close downstream distances at the expense of far distances, where the scan points might not capture enough points inside the deficit and thereby prevent a successful Gaussian fit. Furthermore, additional scan points at the edges can lead to a better representation of the deficit but would also increase the scan time. According to Equation (18), the meandering is correlated to frequencies lower than approximately 0.028 Hz considering a wind speed of 6.5 m/s and a rotor diameter of 117 m. This means that, considering the Nyquist–Shannon sampling theorem, the scan time must be longer than half of the reciprocal of 0.028 Hz, which results in a neccessary scan time of less than 18 s. The scan time for the current usage of 11 scan points is already at about 16 s (depending on the visibility conditions), which is close to the limit of 18 s, so with an increased number of scan points it is no longer ensured that the meandering can be captured.

Figure 9(b) illustrates the wind speed deficit in the ~~MFR~~ HMFR measured under different ambient conditions. The corresponding meandering time series and wind speed deficit for this measured time series at ~~2.96D~~ $2.69D$ downstream is given in Figure A1 in the appendix. The wind shear is fairly high ($\alpha = 0.7$) and the turbulence intensity is very low (~~$I_0 = 2.4\%$~~ $I_0 = 2.4\ \%$). Due to the low turbulence intensity it is still possible to see the w-shape of the wind speed deficit at closer distances. The typical w-shape is caused by the low axial induction in the area of the nacelle. Further downstream, the wake becomes more Gaussian shaped. At a horizontal distance of about ~~1.5D~~ $1.5D$ from the wake center, the wind speed decreases. The reason is ~~probably~~ the wake of other turbines in the wind farm. The mean wind direction in this time series is 183° and the measurements are taken from WTG 1, so it could be either the influence of the wakes of WTG 2 or WTG 4. The associated results of the mean wind speed deficit in the FFR are illustrated in Figure 10. The curves in the FFR are less smooth than the wind speed deficit in the ~~MFR~~HMFR, simply because only 11 points are scanned and no interpolation is necessary when calculating the mean wind speed over the whole time series. Comparing Figures 9 and 10, it becomes apparent that the wind speed deficit in the FFR is less pronounced. Furthermore, for the lower turbulence intensity the w-shape of the wind speed is not visible, since it vanished due to the meandering.

Similar results as exemplarily shown in Figures 9 and 10 have been collected for a multitude of different ambient conditions. The number of measured time series per turbulence intensity and wake generating turbine, on which the LiDAR system is installed, is listed in Table 2. The turbulence intensity is binned in 2° steps. Column 1 of Table 2 specifies the mean values for each bin. Most of the measurement results are collected at low to moderate turbulence intensities (~~$I_0 = (4...10)\%$~~ $I_0 = (4 - 10)\ \%$). Only a few results could be extracted at higher turbulence intensities. The results include time series with an ambient wind speed of 5 m/s to 8 m/s. In this range, both turbines operate under optimal and most efficient conditions resulting in maximum energy output from the wind. The thrust coefficient is constant in this region (see Figure 3). Therefore, the axial induction and the wind speed deficit normalized by the turbine's inflow wind speed are also expected to be constant for similar ambient con-

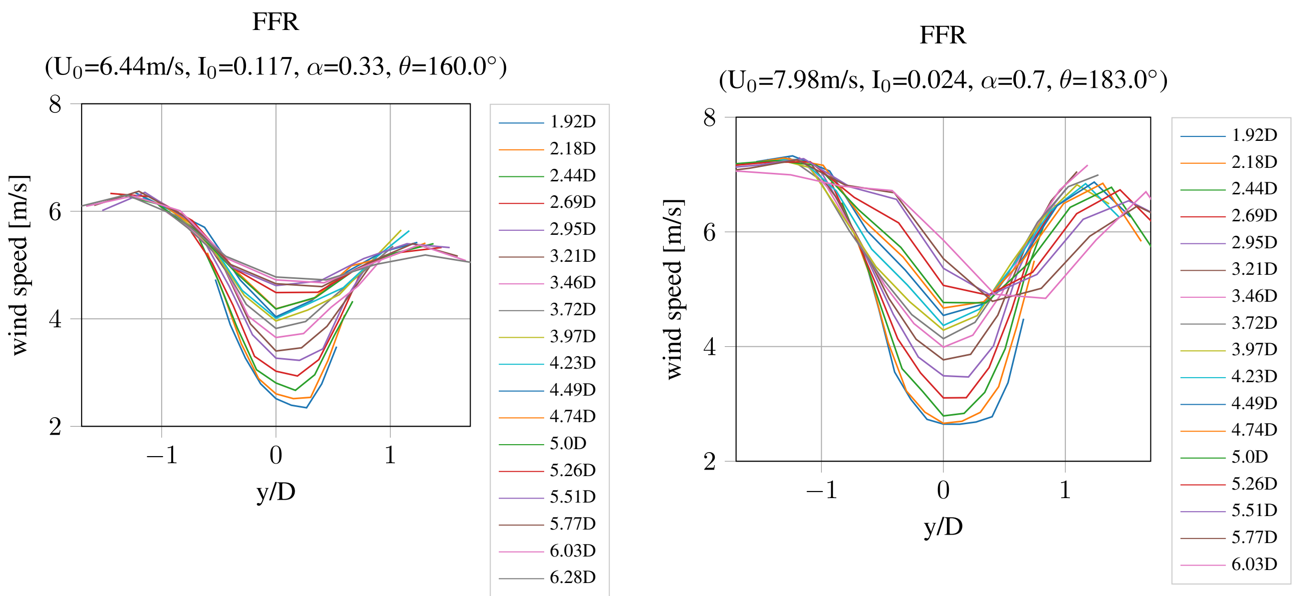

(a)

(b)

Figure 10. Wind speed deficit in the FFR for a turbulence intensity of 11.7 % **(a)** and a turbulence intensity of 2.4 % **(b)**.

Table 2. Number of measured and considered data sets per turbulence intensity for the LiDAR systems on WTG 1 and WTG 2.

I_0 [%]	WTG 1	WTG 2
4	23	28
6	8	11
8	23	14
10	11	9
12	13	4
14	0	0
16	1	1
18	1	2
20	1	3
22	0	2

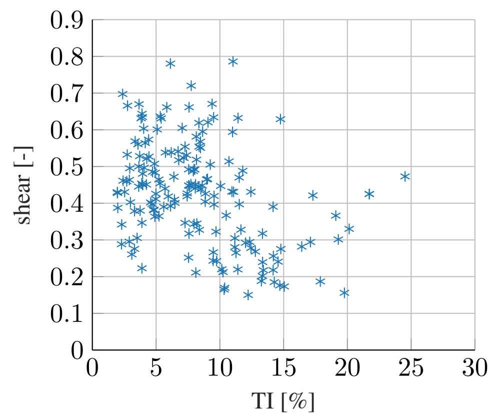

Figure 11. Shear exponenent over the ambient turbulence intensity for all considered data sets.

ditions over this wind speed range. For the single turbulence intensity bins and both turbine types, simulations with different DWM models are carried out applying the same axial induction over the whole wind speed range. A scatterplot of the shear exponent and the ambient turbulence intensity determined by the metmast is given in Figure 11. It includes all used datasets. At lower turbulence intensities, the shear spreads quite a lot, whereas towards higher turbulence intensities the shear decreases as expected.

Figure 12 summarizes all measured wind speed deficits in the ~~MFR.~~ HMFR. It demonstrates the mean value and the

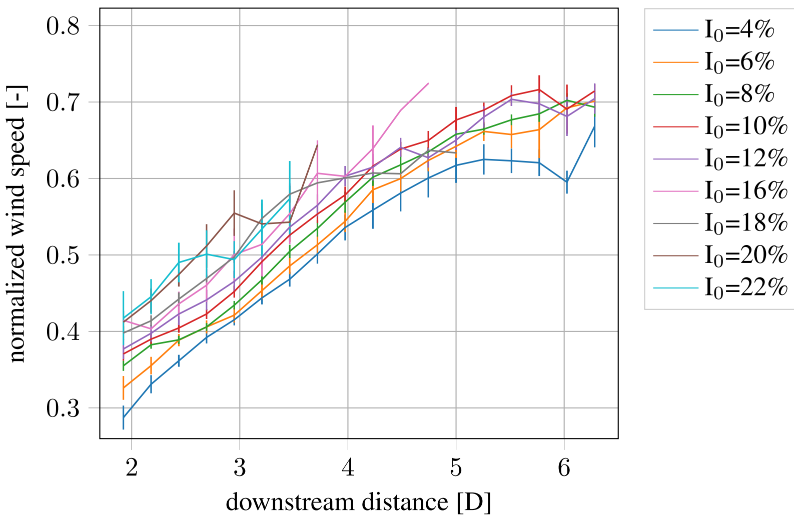

Figure 12. Measured mean value (line) and standard deviation (bar) of the mean value of the minimal wind speed in the HMFR for different turbulence intensity bins with a bin width of 2 %.

standard deviation of the mean for all captured turbulence bins plotted against the downstream distance. Each value is related to the minimum value of the wind speed deficit, which itself is normalized by the inflow wind speed. It should be noted that in some distances only one value satisfies the filtering and plausibility checks, whereby the error bar is omitted. Additionally, it is pointed out that the plotted values always refer to the minimum value of a wind speed curve and not necessarily to the velocity in the wake center. Therefore, no increase of the wind speed at low downstream distances on account of the w-shape is visible. The wind speed deficit at the wake center plotted against the downstream distance is depicted in the next section in Figure 15(b) and will be discussed further at this point. Figure 12 illustrates very well that the lowest degradation of the wind speed deficit occurs at the lowest turbulence intensity. Up to a turbulence intensity of 10 %, the degradation of the wind speed deficit continuously rises, leading to increasing minimum wind speeds at nearly all downstream distances. Above 10 % turbulence intensity, the case is less clear. Especially at larger downstream distances, the measured normalized minimum wind speed happens to fall below the corresponding lower turbulence intensity bin. ~~The most obvious~~ An explanation is the reduced number of measurement results in these bins and the higher uncertainty that comes along with it (expressed as error bars). Furthermore, discrepancies in the determined ambient turbulence intensity at the metmast location and the actual turbulence intensity at the wake position could lead to ~~an~~ a misinterpretation of the LiDAR measurements. ~~Nevertheless, even~~ The farthest distance between the metmast and the location measured by the LiDAR system that occurs in the analyzed sectors is about 1200 m. With an ambient wind speed of 6.5 m/s, this leads to a wake advection time of 185 s, thus even at worst conditions, the measured ambient conditions at the metmast should be valid for the measured wakes from the LiDAR system most of the time. Furthermore, there is no complex terrain at the site, so it can be assumed that the conditions do not change with the wind direction. In addition, the agreement between measurements and simulations is already good in the higher turbulence intensity bins. Thus, the recalibration affects only the lower turbulence intensity bins with larger amounts of data, while the influence of the calibration on higher turbulence intensities is negligible (see Figure 13). Therefore, even though there are some discrepancies, the faster recovery of the wind speed deficit due to the higher ambient turbulence intensity can be verified and the measurements are reliable for the outlined investigation. Thus, it is valid to use these measurement results for ~~a comparison and a~~ comparisons with DWM model simulations and the recalibration of the DWM model in the next section.

8 Comparison between measurements and DWM model simulation

~~Figure 13~~ Figure 13 compares the measured normalized minimum wind speed in the wake to DWM model simulations. The left part of Figure 13 shows results for a relatively low turbulence intensity of 6 %, whereas the right part contains results for a higher turbulence intensity of 16 %. Further results for the remaining turbulence intensity bins are shown in Figures B1 and B2 in the appendix. The simulations were carried out for a specific downstream distance, which corresponds to the center of the range gate of the LiDAR system. It should be noted that the ~~measured wind speeds with~~ wind speeds measured by the LiDAR system can be interpreted as a mean value over the whole range gate. However, the wind speed gradient in axial direction is ~~relatively~~ low and almost linear in the observed ~~donstream~~ downstream distances, so ~~that a fair comparison between simulation~~ even in the DWM model, the discretization in downstream direction is 23.4 m (equivalent to $0.2D$), which is in the same order of the range gate of 30 m. Therefore, a valid comparison between simulations and measurements is carried out. The wind speed deficit simulations in the HMFR obtained by the DWM model also include the vertical meandering to ensure a correct comparison between measurements and simulations. Three different simulation results with varying definitions of the initial deficit and eddy viscosity description are illustrated. The method called “DWM-Egmond” is based on the definitions ~~from~~ of Madsen et al. (2010) and Larsen et al. (2013) and the “DWM-Keck” method is adopted from Keck (2013), see Section 6. ~~It is obvious~~ Figure 13 shows that the DWM-Egmond method overestimates the wind speed deficit ~~over~~ for all downstream distances and for both turbulence intensities. The simulated minimum wind speed with the DWM-Keck method is in better agreement with the measurement results. This confirms the results in Reinwardt et al. (2018). Especially at higher turbulence intensities (Figure 13~~(b)~~), the results of the DWM-Keck model agree very well with the measurements. For lower turbulence intensities and higher distances (greater than ~~3D~~ $3D$) there is a relatively large discrepancy between measurements and simulations. A similar observation was made in Larsen et al. (2013) with the model version in Madsen et al. (2010). Aiming at the adjustment of the simulated degradation of the wind speed deficit in Larsen et al. (2013) for cases like the one presented here, the DWM model has been recalibrated and is henceforth called “DWM-Keck-c” (see Figure 13).

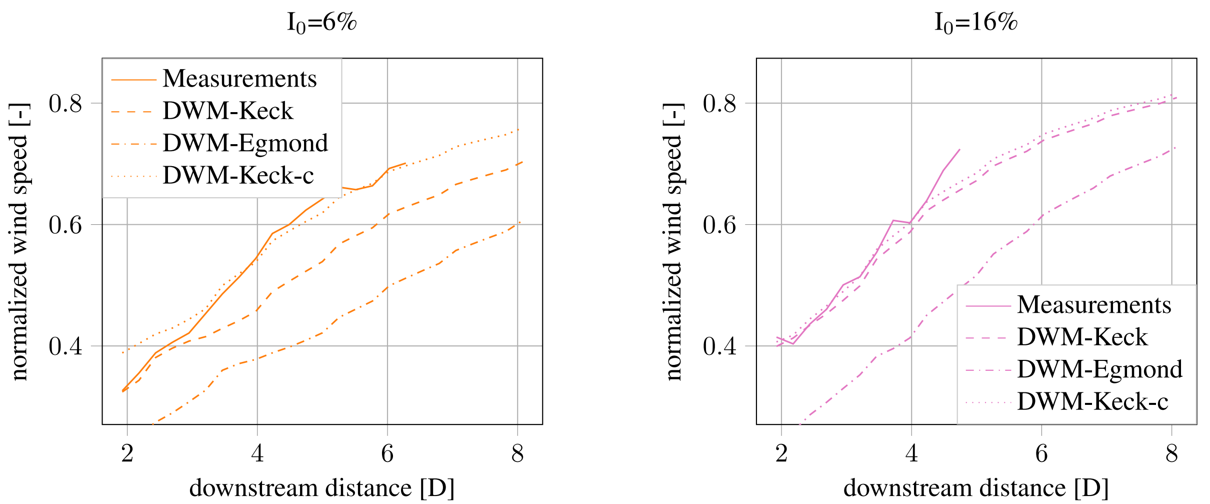

(a) (b)

Figure 13. Comparison of measurements and simulations of the minimum wind speed deficit in the ~~MFR~~ HMFR for different ~~downstream distances~~turbulence intensities. The recalibrated model is denoted DWM-Keck-c.

The recalibration of the DWM model and accordingly the normalized eddy-viscosity definition in the DWM model are based on a least-squares fit of the minimum of the simulated normalized wind speed to the minimum of the measured normalized wind speed for several downstream distances. The definition of the eddy viscosity along with the recalibrated parameters are explained in detail in Section 6.3. For the recalibration the measurement results are divided into 2 % turbulence intensity bins. All measurement results from Figure 12 containing data sets from two different turbines, are used for the recalibration. The first turbine is an N117 turbine with 3 MW and the second one is an N117 with 2.4 MW. DWM model simulations were carried out for both turbine types~~due to the fact that the~~, since the axial induction of both turbines is slightly different under partial load conditions. To calculate a mean value of the simulated minimum wind speed and thus allow a comparison with the results in Figure 12, ~~the simulation results are~~ simulations with both turbine types are carried out for each turbulence intensity bin and weighted in accordance with the number of measurement results per turbine listed in Table 2. Thus, for example at the ambient turbulence intensity bin of 4 %, the mean value of the simulated minimum wind speed consists of the sum of the simulated minimum wind speeds weighted by 0.451 and 0.549, the weighting factors for WTG1 and WTG2, respectively. Nonetheless, this weighting has only a marginal influence on the overall results, because the axial induction in the considered wind speed range (5 m/s to 8 m/s) is very similar for these two turbine types (see also thrust and power curves in Figure 3).

The results of the recalibrated DWM model, denoted Keck-c in Figure 13, coincide very well with the measurements. In particular, the results for lower turbulence intensities could clearly be improved. For higher turbulence intensities, the influence of the recalibration is less significant and the already good agreement between simulation and measurement results remains unchanged. The same applies to the results in the appendix in Figures B1 and B2. Only at the lowest downstream distances and turbulence intensities up to 12 %, the recalibrated model delivers higher deviations than the original model. For downstream distances larger than $3D$, the recalibrated model leads to more than 10 % lower devitaions from the measurements than the original model. For turbulence intensities higher than 16 %, the deviation between the recalibrated and original model is smaller than the uncertainties in the measurements, hence no further conclusions about improvements can be made. The uncertainties in accordance to misalignments could be up to 5 % (see also the data filtering in Section 3). Furthermore, the LOS accuracy of the LiDAR system itself is about 1.5 % at a wind speed of 6.5 m/s. The root-mean-square error (RMSE) between the measured and simulated normalized minimum wind speed is collected for all analyzed turbulence intensity bins in Figure 14. A clear improvement of the results due to the recalibrated model version up to an ambient turbulence intensity of 16 % is visible. For higher turbulence intensity bins, the RMSE of the recalibrated and the original DWM-Keck model version are similar. The DWM-Egmond model delivers significantly higher RMSEs than the other model versions for all turbulence intensity bins. A comparison between the simulated and measured mean wake wind speed over the rotor area has been carried out as well[1]. The improvement of the mean wind speed is less clear in comparison to the normalized minimum wind speed. Yet, there is an improvement or results of equal quality are obtained in almost all turbulence intensity bins. At the tails of the wind speed deficit, the curves are coarse, since less scan points are gathered and the influence of turbulence is much higher (see Figure 9). This leads to an error in the mean wake wind speed but not in the minimum wind speed, which is why the illustration and recalibration of the model are based on the minimum wake wind speed instead of the wake mean wind speed.

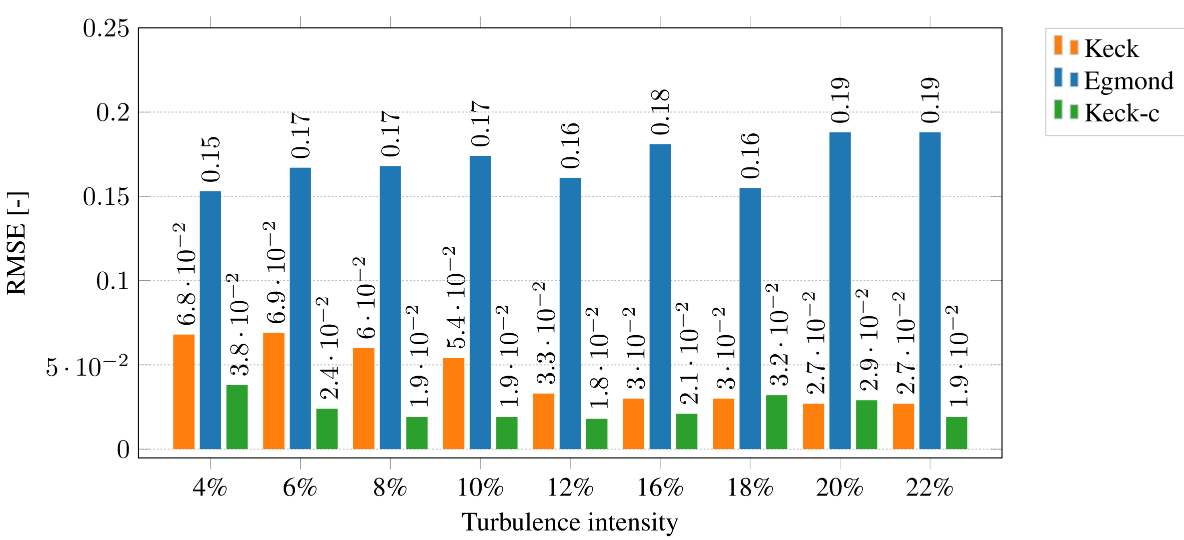

Figure 14. RMSE between the LiDAR measured and the simulated normalized minimum wind speed in the wake.

Figure 15 compares the final recalibrated DWM model to the original model definition. It shows the minimum normalized wind speed (a) and the wind speed at the wake center (b) over downstream distances from ~~0D to 10D~~ $0D$ to $10D$ for the lower and the higher turbulence intensity cases of 6 % and 16 %, respectively. Observing the wind speed at the wake center,

[1] https://www.wind-energ-sci-discuss.net/wes-2019-89/

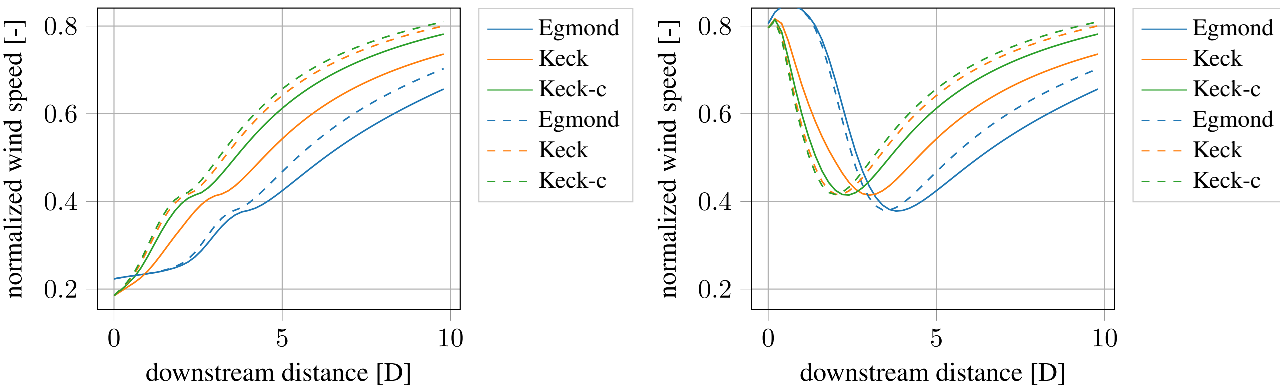

(a) (b)

Figure 15. Simulated minimal normalized wind speed in the MFR **(a)** and normalized wind speed at the wake center **(b)** over the downstream distance for a turbulence intensity of 6 % (solid curves) and 16 % (dashed curves). The recalibrated model is denoted DWM-Keck-c.

higher wind speeds can be seen at lower distances, which derives from the w-shape of the wind speed at these downstream distances. The comparison of the DWM-Keck model (orange curve) and the recalibrated model DWM-Keck-c (green curve) demonstrates that the recalibration leads to a shift of the curve towards lower distances. This shift is more pronounced for the lower turbulence intensity, leading to a faster degradation of the wind speed deficit. For the higher turbulence intensity, both curves, orange and green, are very close to each other over all distances. The faster degradation of the wind speed deficit in the recalibrated model version is caused by introducing the function F_{amb} in the eddy viscosity definition in Equation (21) as explained in Section 6.3. The function increases the eddy viscosity for lower turbulence intensities and thus increases the wind speed deficit degradation in downstream direction. Contemplating the curve of the minimum wind speed in Figure 15(a), small steps are formed in the curves between ~~2D and 4D~~ $2D$ and $4D$ (depending on the used model and the turbulence intensity). These steps correspond to the minimum of the curves in Figure 15(b) and are thus related to the transition from the w-shape of the wind speed deficit towards the Gaussian profile and are consequently caused by the resolution in downstream direction. These steps ~~, visible in Figure 15(a),~~ were also found in some measurements and could likewise be related to the implied transition zone.

9 Conclusions

The study compares measurements of the wind speed deficit with DWM model simulations. The measurement campaign consists of two ~~nacelle mounted~~ nacelle-mounted LiDAR systems in a densely packed onshore wind farm. The LiDAR measurements were prepared ~~with~~ by LiDAR and wind field simulations to ~~determine an optimal scan pattern~~ examine whether the scan pattern is suitable for the outlined analysis. Several wind speed deficits that were simultaneously measured at different downstream distances are presented along with their associated meandering time series. The one-dimensional scan worked reliably in the field campaign, thus, delivering LiDAR data for a multitude of different ambient conditions. These measurements are compared to the simulated wind speed deficit in the ~~MFR~~HMFR. The simulation result of the DWM-Keck model is in good agreement, whereas the DWM-Egmond model yields a too low degradation of the wind speed deficit. Furthermore, even the DWM-Keck model shows some discrepancies to the measurements at low turbulence intensities, which is why a recalibrated DWM model was proposed. The recalibrated model improves the correlation with measurements at low turbulence intensities and leads to ~~a comparably good~~ an agreement at high turbulence intensities~~like~~ , which are as good as the original model, thus ~~,~~ resulting in a very well overall conformity with the measurements.

Future work will include the analysis of two-dimensional scans as well as measurements with more range gates and higher spatial resolutions. Increasing the number of range gates and scan points will lead to ~~higher~~ longer scan times, hence, preventing further analysis of the wind speed deficit in the MFR and the determination of the meandering time series. Nevertheless, a validation of the wind speed deficit in the FFR with higher resolutions and more distances seems reasonable to prove the validity of the outlined calibration also for further distances. Furthermore, the analyzed models will be assessd in load as well as power production simulations and compared ~~with the measured loads in~~ to the particular measurement values from the wind farm. So far, only measured single wakes were presented. Yet, a brief analysis demonstrated that multiple wakes can also be recorded with the described measurement setup. A future step will therefore be an analysis of multiple wake situations.

Code and data availability. Access to LiDAR and metmast data as well as the source code used for post-processing the data and simulations can be requested by the authors.

Author contributions. IR performed all simulations, post-processed and analyzed the measurement data and wrote the paper. LS and DS gave technical advice in regular discussions and reviewed the paper. PD and MB reviewed the paper and supervised the investigations.

Competing interests. The authors declare that they have no conflict of interest.

Acknowledgements. The content of this paper was developed within the project NEW 4.0 (North German Energy Transition 4.0), which is funded by the Federal Ministry for Economic Affairs and Energy (BMWI).

Appendix A: Measurement results

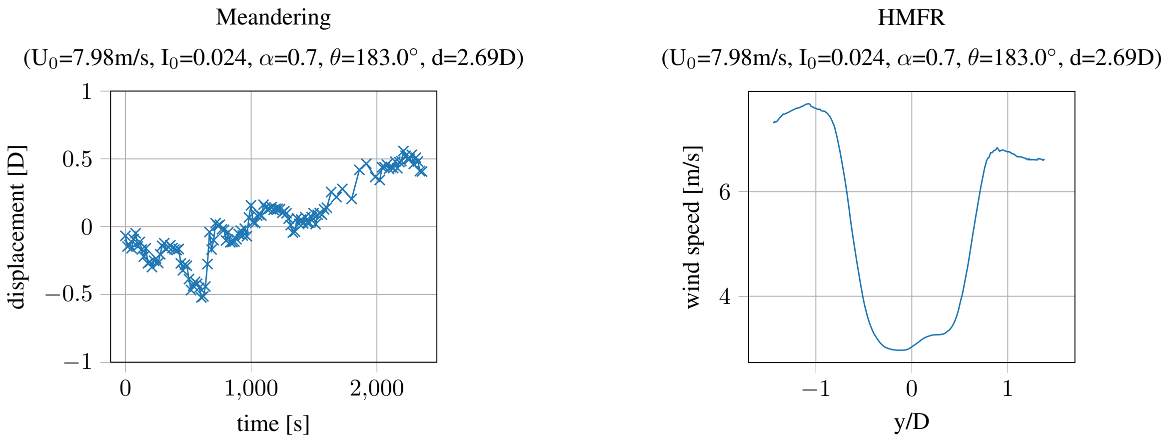

(a) (b)

Figure A1. Meandering time series **(a)** and wind speed deficit in the ~~MFR~~ HMFR **(b)** at ~~2.69D~~ $2.69D$ downstream of the turbine.

Appendix B: Comparison of measurements and DWM model simulation

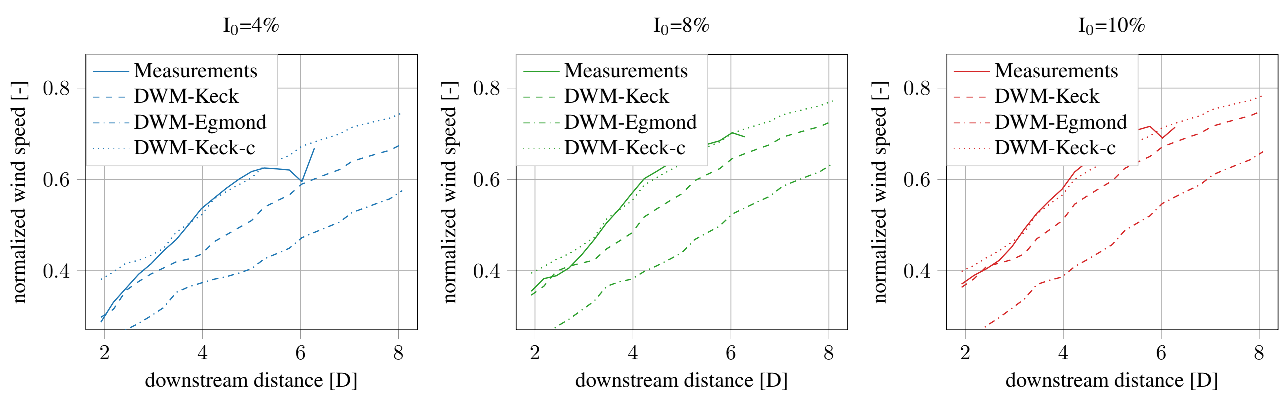

(a) (b) (c)

Figure B1. Comparison of measurements and simulations of the minimum wind speed deficit in the ~~MFR~~ HMFR for different ~~downstream distances~~turbulence intensities. The recalibrated model is denoted DWM-Keck-c.

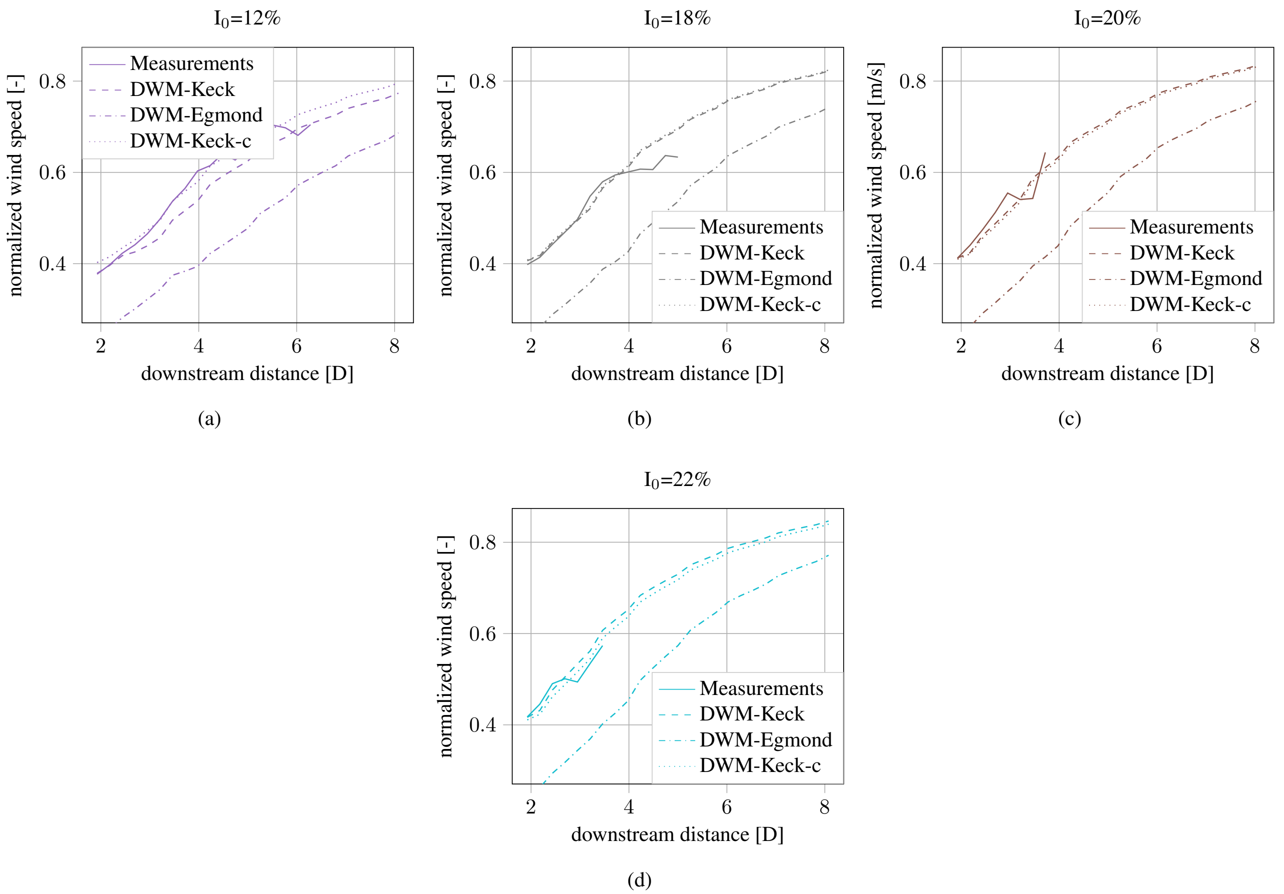

Figure B2. Comparison of measurements and simulations of the minimum wind speed deficit in the ~~MFR~~ HMFR for different ~~downstream distances~~turbulence intensities. The recalibrated model is denoted DWM-Keck-c.

References

Ainslie, J. F.: Calculating the flowfield in the wake of wind turbines, J. Wind Eng. Ind. Aerodyn., 27, 213–224, 1988.

Bingöl, F., Mann, J., and Larsen, G. C.: Light detection and ranging measurements of wake dynamics Part I: One-dimensional scanning, Wind Energy, 13, 51–61, https://doi.org/10.1002/we.352, 2010.

Frandsen, S.: Turbulence and turbulence-generated structural loading in wind turbine clusters, Ph.D. thesis, Technical University of Denmark, 2007.

Gerke, N., Reinwardt, I., Dalhoff, P., Dehn, M., and Moser, W.: Validation of turbulence models through SCADA data, JPCS, 1037, 072 027, https://doi.org/10.1088/1742-6596/1037/7/072027, 2018.

IEC 61400-1 Ed.4: IEC 61400-1 Ed. 4: Wind energy generation systems - Part 1: Design requirements, Guideline, International Electrotechnical Commission (IEC), 2019.

Keck, R.-E.: A consistent turbulence formulation for the dynamic wake meandering model in the atmospheric boundary layer, Ph.D. thesis, Technical University of Denmark, 2013.

Keck, R.-E., de Maré, M., Churchfield, M. J., Lee, S., Larsen, G., and Madsen, H. A.: On atmospheric stability in the dynamic wake meandering model, Wind Energy, 17, 1689–1710, 2014.

Larsen, G. C., Madsen, H. A., Bingöl, F., Mann, J., Ott, S. r., Sørensen, J. N., Okulov, V., Troldborg, N., Nielsen, M., Thomsen, K., Larsen, T. J., and Mikkelsen, R.: Dynamic wake meandering modeling, Tech. Rep. Risø-R-1607(EN), Risø National Laboratory, 2007.

Larsen, G. C., Madsen, H. A., Larsen, T. J., and Troldborg, N.: Wake modeling and simulation, Tech. Rep. Risø-R-1653(EN), Risø National Laboratory for Sustainable Energy, 2008a.

Larsen, G. C., Madsen, H. A., Thomsen, K., and Larsen, T. J.: Wake meandering: A pragmatic approach, Wind Energy, 11, 377–395, https://doi.org/10.1002/we.267, 2008b.

Larsen, T. J., Madsen, H. A., Larsen, G. C., and Hansen, K. S.: Validation of the dynamic wake meander model for loads and power production in the Egmond aan Zee wind farm, Wind Energy, 16, 605–624, 2013.

Machefaux, E., Troldborg, N., Larsen, G., Mann, J., and Aagaard Madsen, H.: Experimental and numerical study of wake to wake interaction in wind farms, in: Proceedings of EWEA 2012 - European Wind Energy Conference & Exhibition, European Wind Energy Association (EWEA), 2012.

Machefaux, E., Larsen, G. C., Troldborg, N., and Rettenmeier, A.: Single wake meandering, advection and expansion - An analysis using an adapted pulsed lidar and CFD LES-ACL simulations, in: Prodeedings of EWEA 2013 - European Wind Energy Conference & Exhibition, European Wind Energy Association (EWEA), 2013.

Machefaux, E., Larsen, G. C., Troldborg, N., Gaunaa, M., and Rettenmeier, A.: Empirical modeling of single-wake advection and expansion using full-scale pulsed lidar-based measurements, Wind Energy, 18, 2085–2103, https://doi.org/10.1002/we.1805, 2015.

Machefaux, E., Larsen, G. C., Troldborg, N., Hansen, K. S., Angelou, N., Mikkelsen, T., and Mann, J.: Investigation of wake interaction using full-scale lidar measurements and large eddy simulation, 19, 1535–1551, https://doi.org/10.1002/we.1936, 2016.

Madsen, H. A., Larsen, G. C., Larsen, T. J., and Troldborg, N.: Calibration and validation of the dynamic wake meandering model for implementation in an aeroelastic code, J. Sol. Energy Eng., 132, 041 014, 2010.

Reinwardt, I., Gerke, N., Dalhoff, P., Steudel, D., and Moser, W.: Validation of wind turbine wake models with focus on the dynamic wake meandering model, JPCS, 1037, 072 028, https://doi.org/10.1088/1742-6596/1037/7/072028, 2018.

Trujillo, J.-J., Bingöl, F., Larsen, G. C., Mann, J., and Kühn, M.: Light detection and ranging measurements of wake dynamics. Part II: Two-dimensional scanning, Wind Energy, 14, 61–75, https://doi.org/10.1002/we.402, 2011.

Veers, P. S.: Three-Dimensional Wind Simulation, Tech. Rep. SAND88-0152(EN), Sandia National Laboratories, 1988.